Reviews in Mineralogy & Geochemistry
Vol. 89 pp. 207-241, 2023

Lunar Magnetism

Mark A. Wieczorek[1], Benjamin P. Weiss[2], Doris Breuer[3], David Cébron[4], Mike Fuller[5], Ian Garrick-Bethell[6,7], Jérôme Gattacceca[8], Jasper S. Halekas[9], Douglas J. Hemingway[10], Lon L. Hood[11], Matthieu Laneuville[12], Francis Nimmo[6], Rona Oran[2], Michael E. Purucker[13], Tina Rückriemen[3], Krista M. Soderlund[14], Sonia M. Tikoo[15]

[1]*Observatoire de la Côte d'Azur, Laboratoire Lagrange, Nice, France*
[2]*Department of Earth, Atmospheric and Planetary Sciences, Massachusetts Institute of Technology, Cambridge, Massachusetts, USA*
[3]*Institute for Planetary Research, German Aerospace Center (DLR), Berlin, Germany*
[4]*ISTerre, Université Grenoble-Alpes, CNRS, Grenoble, France*
[5]*University of California, Santa Barbara, California, USA*
[6]*University of California, Santa Cruz, California, USA*
[7]*Kyung Hee University, Yongin, Gyeonggi 446-701, Korea*
[8]*Aix-Marseille Université, CNRS, IRD, Collège de France, INRAE, CEREGE, Aix-en-Provence, France*
[9]*University of Iowa, Iowa City, Iowa, USA*
[10]*University of California, Berkeley, California, USA*
[11]*Lunar and Planetary Laboratory, University of Arizona, Tucson, USA*
[12]*Earth-Life Science Institute, Tokyo Institute of Technology, Meguro, Tokyo, Japan*
[13]*NASA Goddard Space Flight Center, Greenbelt, Maryland, USA*
[14]*Institute for Geophysics, Jackson School of Geosciences, University of Texas at Austin, Austin, Texas, USA*
[15]*Department of Geophysics, Stanford University, Stanford, California, USA*

mark.wieczorek@oca.eu

1. INTRODUCTION

Analyses of lunar rocks and magnetic field data from orbit show that the Moon once had a global magnetic field generated by an internal dynamo. Magnetization of the deep crust implies that a dynamo operated during the first 100 million years following crust formation and magnetization of some impact basins implies that the dynamo continued into the Nectarian period. Paleomagnetic analyses of Apollo samples provide evidence for dynamo activity from about 4.25 billion years ago (Ga) until at least 1.92 Ga, ceasing thereafter by ~0.80 Ga. The field strength was Earth-like until about 3.56 Ga (from ~40 to 110 μT), after which it decreased by more than an order of magnitude. Several mechanisms have been proposed to account for the long duration of the lunar dynamo. These include thermal convection in the core that could power a dynamo for a few hundred million years, core crystallization that could power a dynamo until about 1.5 Ga, mantle and/or inner core precession that could power a dynamo beyond 2 Ga, impact-induced changes in the rotation rate of the mantle that could power several short-lived dynamos up until when the last basin formed at ~3.7 Ga, and a basal magma ocean that could have potentially powered a dynamo over much of lunar history.

1529-6466/23/0089-0005$05.00 (print)
1943-2666/23/0089-0005$05.00 (online)
http://dx.doi.org/10.2138/rmg.2023.89.05

Magnetohydrodynamic simulations have shown that the amplification of pre-existing fields by impact generated plasmas are insufficient and too short lived to have played an important role in crustal magnetization. Some of the magnetic carriers responsible for crustal magnetization, such as those responsible for the magnetization of the deep highland crust and mare basalts, are of lunar origin. Other magnetic carriers may instead be derived from meteoritic materials that were accreted to the Moon during large impacts. Outstanding questions in lunar magnetism include the geometry of the internally generated magnetic field, the exceedingly high surface field strengths implied by some paleomagnetic analyses, whether dynamo activity was continuous or episodic, the origin of strong crustal magnetic anomalies that have no correlation with surface geology, and the mechanisms that powered the lunar dynamo through time.

Portions of the Moon's crust were magnetized in the presence of magnetic fields in the distant past, and the origin of these magnetized materials are intertwined with many aspects of the Moon's complex geologic evolution. If the magnetizing field was a global field generated by dynamo processes in the core of the Moon, the strength and duration of the dynamo field would be closely related to the core's size, its composition, and its cooling history. The magnetization recorded in lunar rocks is related not only to the strength of the magnetizing field, but also to the properties and abundances of the magnetic minerals in these rocks and the processes by which they became magnetized. Some questions about lunar magnetism can be addressed by studying the present-day strength of the magnetic field, either from orbit or on the surface. Other questions require the use of laboratory analyses of actual rocks that were magnetized on the Moon. And yet others require numerical modeling to understand the processes that can lead to an internal dynamo.

Of all the terrestrial bodies in our solar system, magnetic investigations of the Moon have been surpassed only by those of Earth. Prior to the Apollo missions, spacecraft observations by Luna 2, Luna 10 and Explorer 35 demonstrated that the Moon did not have a significant global magnetic field (e.g., Dolginov et al. 1966; Sonett et al. 1967). The initial studies of lunar rocks returned by the Apollo 11 mission, however, showed that some samples did carry a paleomagnetic record. Metallic iron and iron-nickel were identified to be the principal magnetic carriers, and this caused difficulties for traditional paleomagnetic methods that had been developed to analyze the iron oxides more common on Earth. Low altitude orbital measurements were made later during the Apollo 15 and 16 missions, showing that the lunar crust was heterogeneously magnetized. Magnetometer measurements were made on the surface of the Moon during 4 Apollo missions (Dyal et al. 1974) and from the later Lunokhod 2 rover (Dolginov et al. 1976). The portable magnetometer measurements showed that the surface field directions changed dramatically over km length scales.

At the close of the Apollo era, the study of lunar magnetism provided several important insights concerning lunar evolution, but also left some fundamental questions unresolved. Both the paleomagnetism and orbital measurements implied that strong magnetic fields once existed on the surface of the Moon, but the origin of these fields was debated. Although many interpreted the measurements as evidence for an ancient lunar dynamo, others emphasized that transient fields generated or amplified by plasmas from meteoroid impacts could explain some of the paleomagnetic record. The paleointensity results appeared to indicate an era of strong fields (tens of μT) near 3.8–3.9 Ga, but the time evolution of the field strength was complicated by the limited age range of the samples that were investigated, the observation that some young samples appeared to be magnetized, and the observation that the field strengths were variable for any given time period. No detailed dynamo models were published at this time, and it was difficult to understand how the small size (<400 km) of the lunar core could generate surface field strengths comparable to that of Earth. Lastly, the origin of the materials responsible for the magnetic anomalies observed from orbit were not understood. Though some anomalies appeared to be related to impact processes, others had no clear correlation with lunar geologic processes.

Previous reviews have focused on the results of the Apollo-era paleomagnetic investigations (Strangway et al. 1973; Fuller 1974; Fuller and Cisowski 1987) and the Apollo-era magnetometer measurements (Dyal et al. 1974; Schubert and Lichtenstein 1974; Hood 1986). At the time when the *New Views of the Moon* book was written in 2006, no major advancements in lunar paleomagnetism studies had been made in nearly two decades. Although it was fairly well established by then that the Moon does indeed possess an iron core that is today partly liquid (e.g., Wieczorek et al. 2006), there was no agreement that the Moon had generated a dynamo magnetic field. In particular, the possibility existed that lunar paleomagnetism was the product of exogenous field sources like impact-generated plasmas. Since this time, several major advances have occurred. First, paleomagnetic studies of lunar samples have experienced a renewed interest. Second, global magnetic field models have become available using data acquired by the Lunar Prospector and Kaguya missions. Lastly, there have been several investigations of dynamo generation in the Moon's metallic core or potentially in a basal silicate magma ocean. Collectively, these new data and models have now confidently established that the ancient Moon generated a dynamo magnetic field.

The status of lunar magnetism was last reviewed by Weiss and Tikoo in 2014, who emphasized the recent results from paleomagnetism studies and dynamo models. In this chapter, we review the advances that have been made in all fields of lunar magnetism over the past two decades and discuss several important developments that have occurred since the last review. We begin in Section 2 by describing recent lunar paleomagnetism studies performed using modern analysis techniques. These studies improve our understanding of the magnetization process, quantify the role of the various forms of possible remanent magnetization, and provide improved estimates for the time evolution of the surface field strength. In Section 3, we review results made possible by new global magnetic field models of the Moon. These global datasets constrain the role of impact events in crustal magnetism, place constraints on the origin and timing of crustal magnetization, and also constrain the global field geometry and how it might have varied over time. In Section 4, we review the various models that have been proposed for powering a lunar dynamo. These models include early thermal convection in the core or a basal magma ocean, thermo-compositional convection driven by core crystallization, mechanical forcing by precession of the solid mantle and/or solid inner core, and inertial instabilities generated by changes in the rotation rate of the mantle following large impact events. In Section 5, we synthesize the paleomagnetism, crustal magnetism, and dynamo studies and discuss the time evolution of the lunar dynamo and the origin of crustal magnetism. Finally, we summarize in Section 6 the remaining problems in lunar magnetism and provide guidance for future studies.

2. PALEOMAGNETISM

Paleomagnetic analyses of lunar samples constrain the past surface magnetic field of the Moon. In this section, we review the magnetic properties of lunar rocks, summarize the mechanisms by which lunar rocks can be magnetized, and describe the methods that are used for paleointensity determination. Finally, we summarize the results of modern paleointensity studies of Apollo samples.

2.1. Lunar magnetic mineralogy

Lunar rocks formed under highly reducing conditions compared to the Earth's interior, with mare basalts having oxygen fugacities about a factor of 10 below that of the iron-wüstite buffer. As a result, the dominant ferromagnetic minerals in lunar rocks are in the form of the body-centered cubic metallic iron–nickel minerals kamacite (α-$Fe_{1-x}Ni_x$ for $x \lesssim 0.05$) and martensite (α_2-$Fe_{1-x}Ni_x$ for $\sim 0.05 < x \lesssim 0.25$), and the iron phosphide mineral schreibersite $(Fe_{1-x}Ni_x)_3P$ with $x \sim 0.1$, rather than the iron oxides and sulfides that dominate the Earth's crust (Fuller and Cisowski 1987; Rochette et al. 2010). These minerals could have formed either during crystallization of

endogenous lunar melts, by subsolidus reduction of oxides, sulfides, and silicates (thought to be due to implantation of solar wind hydrogen followed by metamorphism and/or impact melting), or by meteoritic contamination at the lunar surface (Heiken et al. 1991; Rochette et al. 2010).

There are three principal difficulties in studying the paleomagnetism of lunar rocks. First, the size ranges in which Fe metal minerals form magnetically stable single domain crystals is very narrow: 10–70 nm for elongate grains with ratios of width to length >0.5 (Muxworthy and Williams 2015), and almost non-existing for equant grains. Single domain grains are desirable because they can retain ancient natural remanent magnetization (NRM) that is stable against viscous demagnetization due to residing at ambient lunar surface temperatures for >4 billion years (Garrick-Bethell and Weiss 2010) and against remagnetization by stray fields during sample transport and handling. By comparison, larger multidomain grains are problematic because they are more easily remagnetized and because their magnetization may not be thermally stable over solar system history. In many cases, it may be difficult to isolate primary magnetization signals formed during initial cooling of the rocks on the Moon from secondary contaminating magnetic overprints in multidomain grains (although see Berndt and Chang 2018). Because the size range of multidomain grains is so vast ($\gtrsim$20–70 nm depending on grain shape), most lunar rocks tend to be dominantly multidomain and therefore are nonideal for paleomagnetic studies. However, this problem has been partially mitigated by the realization that grains with diameters up to several hundred nm, which form modestly nonuniform magnetic structures known as single and multiple-vortex states, also can carry magnetization that is stable over billions of years, can be thermally cleaned of magnetic overprints, and can accurately record the intensity of past magnetic fields (Almeida et al. 2016; Einsle et al. 2016; Nagy et al. 2019).

The second difficulty arises because paleointensity determinations classically involve heating rocks to high temperatures (up to ~780 °C for lunar rocks, see Section 2.3). Lunar metallic minerals will rapidly oxidize during heating in the Earth's atmosphere which has an oxygen fugacity 21 orders of magnitude higher than that of lunar rocks at 500 °C. This can happen at just 200–300 °C, destroying the magnetic records and rendering paleointensity determinations inaccurate. This led to the widespread use of room-temperature alternating field (AF) demagnetization as an alternative method for removing magnetic overprints from lunar rocks. However, the multidomain sizes of most lunar metal grains makes them highly susceptible to acquiring magnetic contamination known as spurious anhysteretic remanent magnetization (ARM) during AF demagnetization (ARM forms when a rock is exposed to a strong alternating field of decreasing intensity in the presence of a static bias field).

The third problem is that martensite (but not kamacite) will transform to the face-centered cubic mineral taenite (γ-FeNi) during laboratory heating above a characteristic austenite-start temperature and then reform back to martensite during cooling below a lower characteristic martensite-start temperature (Swartzendruber et al. 1991). For grains with >10 atomic % nickel content, these temperatures are each sufficiently low (<700 °C and <500 °C, respectively) that magnetization acquired during primary cooling on the Moon will not be a pure thermoremanent magnetization (TRM), but will also contain a significant contribution from crystal growth known as thermochemical remanent magnetization (TCRM). There are no known laboratory techniques designed to accurately retrieve paleointensity measurements from rocks with TCRM.

2.2. Acquisition of magnetization

Three conditions are required for rocks to acquire a remanent magnetization: the presence of ferromagnetic minerals in the rock, the existence of an ambient magnetic field, and the occurrence of a magnetizing event. For a single magnetizing event, the acquired NRM in A m^{-1}, as given by the variable M can be expressed as

$$M = fM_{rs}B \tag{1}$$

where B is the ambient magnetic field in units of Teslas (T) at the time of magnetization acquisition, M_{rs} is the saturation remanence in units of A m^{-1} (which can be measured in the laboratory and is often abbreviated as SIRM), and f is an efficiency parameter with units of T^{-1} that depends on the magnetizing process. When working with samples, magnetizations are usually reported per unit mass (as opposed to volumetrically) and are given in units of A m^2 kg^{-1}.

Lunar rocks can acquire NRM through a variety of processes: on the Moon, TRM can be acquired when Fe–Ni with Ni≲5 atomic % cools from 780 °C or lower in the presence of a magnetic field. Partial TRM (pTRM) can be the result of later reheating at lower temperatures. Shock remanent magnetization (SRM) can be the result of shock waves created by hypervelocity impacts (Gattacceca et al. 2010). TCRM can form during cooling for Fe–Ni with Ni≳10 atomic% (see above). Other remanences can be acquired after collection on the Moon as a result of sample handling. Isothermal remanent magnetization (IRM) can be acquired if rocks are exposed to strong (≳ 1 mT) fields (Pearce et al. 1976; Garrick-Bethell et al. 2009). Viscous remanence (VRM) is unavoidably acquired as a result of long-term exposure to the geomagnetic field. pTRM may be acquired if samples are cut with a band saw or circular saw without lubricants that results in local heating of the cut faces (Tikoo et al. 2014; Mighani et al. 2020). These contaminating remanences can partially or totally erase older magnetizations.

Retrieving the paleofield B requires the identification and removal of magnetic contamination, the identification of the natural magnetization process(es), and the calibration of the efficiency factor f for the given process. Identification of the magnetization process can help constrain the age of the NRM, which can differ from the crystallization age of the sample. As shown in Figure 1, this can be achieved from petrography and thermochronology by comparing the thermal or AF stepwise demagnetization behavior of the NRM with that of analog magnetizations imparted in the laboratory (e.g., Fuller and Cisowski 1987; Shea et al. 2012). TRM can be simulated in the laboratory by heating the sample to above its maximum blocking temperature and cooling in a known magnetic field. Because heating experiments often result in chemical alteration of lunar rocks, isothermal ARM can be used as an analog (Stephenson and Collinson 1974). pTRM can be simulated by heating a sample to a given temperature lower than the maximum blocking temperature. SRM can be simulated using a quasi-hydrostatic pressure cell and laser shocks in controlled magnetic fields (Gattacceca et al. 2010). IRM can be simulated by applying a strong magnetic field to the sample (such as SIRM), and VRM can be simulated by keeping the sample in a low magnetic field during long periods of time (days to months).

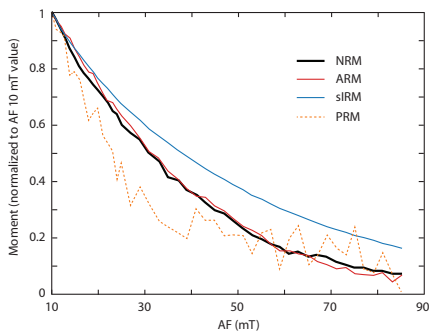

Figure 1. Intensity of natural remanent magnetization (NRM) and various laboratory-induced magnetizations as a function of AF demagnetization level for a sample of mare basalt 10017 (data from Suavet et al. 2013). Anhysteretic remanent magnetization (ARM) is an analogue to thermoremanent magnetization (TRM). Piezoremanent magnetization (PRM) is an analogue to shock remanent magnetization (SRM). Saturation isothermal remanent magnetization (SIRM) simulates exposure of the sample to strong magnetic fields. Intensities are normalized to the 10 mT step that corresponds to the start of the high coercivity component isolated in this rock. The demagnetization behavior of this sample is most similar to that of ARM, and the high coercivity component is interpreted as a TRM acquired during cooling on the Moon.

Because lunar rock storage facilities do not offer protection from the geomagnetic field, all lunar samples have acquired a VRM since their return from the Moon. Because of the typical logarithmic rate of VRM acquisition (and decay) with time, the VRM acquired on Earth for a sample remaining in the same position for 50 years typically can be reduced by 70% over one month of storage in a near-zero field. VRM contamination, being a thermally activated process, is best removed by thermal demagnetization (heating for 1 hour to $\gtrsim 125\,^{\circ}\mathrm{C}$ for single domain grains; Garrick-Bethell and Weiss 2010). VRM contamination can thus be rather easily quantified and mitigated. IRM contamination is more problematic because of the generally low coercivity of lunar rocks. Because the recording of IRM is dependent on coercivity, it is more effectively removed by AF demagnetization and can be identified by a high ratio of NRM to IRM over the lower coercivity range of the NRM (e.g., Gattacceca and Rochette 2004). IRM contamination has been recognized in a number of lunar rocks and likely originated at least in part by exposure to magnetic fields in the spacecraft during the return trip from the Moon (Pearce et al. 1973).

2.3. Paleointensity methods

The origin of the field that magnetized the lunar samples could be constrained by determining both the intensity and direction of the magnetizing field. Given that virtually all Apollo samples were collected as unoriented regolith fragments, lunar paleomagnetic studies have focused almost exclusively on obtaining paleointensities rather than paleo-directions.

Since all paleointensity methods are designed for rocks containing TRM, lunar paleomagnetic studies should target samples that contain a primary TRM. One such rock, as demonstrated in Figure 2, is the melt glass matrix of regolith breccia 15498. As demonstrated in this figure, the TRM is unidirectional throughout the rock (Fig. 2a) and stable in direction during laboratory heating to high temperatures (Fig. 2b). The direct proportionality between TRM and ambient field strength provides the basis for the laboratory double heating-based paleointensity method of Thellier and Thellier (1959). Variants of this approach are now among the standard techniques used in terrestrial paleointensity studies since they can enable the most accurate paleointensity estimates for samples containing a TRM (assuming thermochemical alteration during the laboratory experiment is minimal). During such experiments, a sample is stepwise alternately heated to increasing temperatures in a zero-field environment to demagnetize a fraction of the NRM, ΔNRM, and heated in a known field B_{lab} at the same temperature steps to impart the sample with a laboratory TRM, ΔTRM (see Fig. 2c). Assuming that no thermochemical alteration to the ferromagnetic grains has occurred, the paleointensity may be deduced from the equation

$$B_{\mathrm{paleo}} = \frac{\Delta \mathrm{NRM}}{\Delta \mathrm{TRM}} B_{\mathrm{lab}} \tag{2}$$

Because laboratory heating can thermochemically alter lunar rocks, a range of methods have been utilized in the past to mitigate alteration. Several studies tried heating samples in a vacuum (e.g., Dunn and Fuller 1972; Gose et al. 1973; Lawrence et al. 2008), sometimes using a titanium getter to dehydrate samples prior to heating (e.g., Sugiura and Strangway 1980, 1983). Others tried heating samples in pure Ar (Sugiura et al. 1978) or H_2 diluted into N_2. However, these efforts were largely unsuccessful because they produced environments that were either too oxidizing or too reducing compared to the lunar interior and surface.

A recent major advance is the development of controlled atmosphere thermal demagnetization systems that can heat and cool lunar rocks under lunar oxygen fugacity conditions (Suavet et al. 2014; Tikoo et al. 2017; Mighani et al. 2020). Using mixtures of CO_2 and H_2, the oxygen fugacity can be independently controlled as a function of temperature, thereby mitigating the oxidation-reduction reactions that have plagued lunar thermal paleointensity analyses for the last five decades. Although such systems still do not address the transformation of martensite to austenite that occurs during laboratory heating, they have

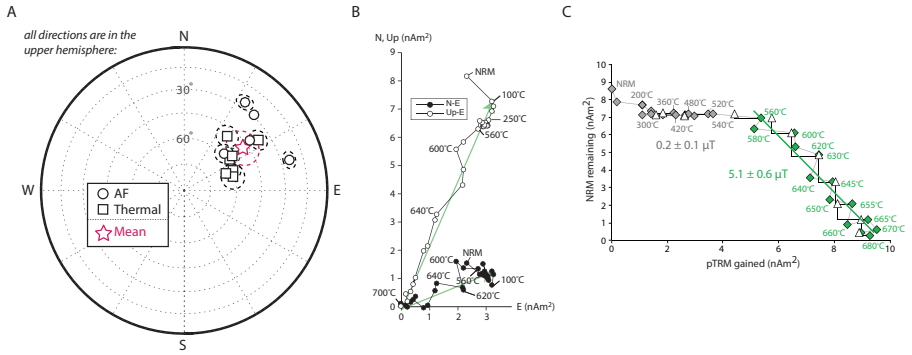

Figure 2. Paleomagnetism of the young (1.47±0.45 Ga) lunar regolith breccia 15498, which demonstrates the protracted lifetime of the lunar dynamo. (**A**) Equal-area stereographic projection showing primary magnetization component directions from 12 mutually oriented glassy subsamples. AF and thermally demagnetized subsamples are displayed using **circles** and **squares**, respectively, with surrounding ellipses representing the associated uncertainty estimates. The mean direction and 95% confidence interval are shown by the **red star** and **ellipse**, respectively. (**B**) Vector endpoint diagram showing zero-field thermal demagnetization steps for subsample 313e. The primary magnetization component is isolated after heating to ~500 ºC. (**C**) Controlled atmosphere Thellier–Thellier paleointensity experiment on subsample 313e. Shown is the NRM lost during progressive thermal demagnetization versus laboratory partial TRM gained over the sample demagnetization interval. Partial TRM checks for alteration are shown as triangles; the partial TRM gained during these steps lie within 20% of that for the previous measurements at the same temperature interval, consistent with the lack of major sample thermochemical alteration during the experiment. **Gray segments** link consecutive thermal steps. Paleointensities for the temperature ranges of 250–540 °C and 560–680 °C are denoted with **dark gray** and **green symbols**, respectively. The paleointensity of 5.1±0.6 μT for the higher temperature range is interpretted as the surface field strength when the rock formed. Figure modified from Tikoo et al. (2017).

now enabled double heating paleointensity measurements of several lunar rocks whose quality is comparable to those of many Earth rocks.

Due to the aforementioned difficulties, lunar paleointensity studies have mostly employed non-heating methods to avoid thermochemical alteration. In these methods, the NRM of the sample is first characterized using AF demagnetization. Afterward, the same sample is either imparted with laboratory ARM or a saturation isothermal remanent magnetization (SIRM) as proxies for TRM. Paleointensities from the ARM method are calculated using

$$B_{\text{paleo}} = \frac{\Delta\text{NRM}}{\Delta\text{ARM}} \cdot \frac{B_{\text{bias}}}{f'} \tag{3}$$

where ΔNRM and ΔARM are respectively the NRM and ARM lost during an AF demagnetization step, B_{bias} is the magnitude of the DC bias field, and f' is a calibration factor determined from independent laboratory studies (Stephenson and Collinson 1974). For samples with multidomain kamacite grains, an average value of f' of ~1.31 has typically been used (Weiss and Tikoo 2014). However, the f' values appear to be log-normally distributed and it would perhaps be better to use the geometric mean of 1.30 and the geometric (multiplicative) standard deviation of 1.18.

Paleointensities can also be deduced using the ratio of NRM lost during AF demagnetization to the saturation isothermal remanent magnetization ΔSIRM lost over the same peak field interval from the relationship

$$B_{\text{paleo}} = a\frac{\Delta\text{NRM}}{\Delta\text{SIRM}} \tag{4}$$

The calibration constant *a* varies with grain shape and grain size, and modern paleomagnetic studies have typically utilized a value equal to 3000 μT (Kletetschka et al. 2003; Gattacceca and Rochette 2004). A recent review of the calibration data for FeNi-bearing samples gives a mean value of 2810 μT for multidomain samples and 3770 μT for single-domain and pseudo-single-domain samples (Weiss and Tikoo 2014). As the calibration data appear to be log-normally distributed, it is perhaps more appropriate to use the geometric means, which are respectively 2070 μT for multidomain samples and 3420 μT for single domain and pseudo-single domain samples, with geometric (multiplicative) uncertainties of 2.2 and 1.7, respectively. An alternative approach has been developed by Kletetschka et al. (2004) and Kletetschka and Wieczorek (2017) that involves normalizing the SIRM by the saturation magnetization of the magnetic carrier. However, this method yields *a* values 3 times larger than quoted above for rocks that contain metallic iron. The origin of this discrepancy has yet to be resolved.

2.4. Paleointensity results

Apollo-era paleointensity measurements provided early evidence that lunar rocks recorded high (≥50 μT) lunar surface fields from ~3.9 to ~3.7 Ga followed by a period of lower field intensities that may have lasted until sometime between 3.6 Ga (Fuller 1998) and the present (Runcorn 1996). This trend is also observed when comparing the ratios of raw NRM intensities to magnetic susceptibilities (a protocol that provides a very crude paleointensity estimate) for Apollo samples of different ages (Lepaulard et al. 2019). However, these studies were limited by the low recording fidelity of most lunar rocks, the lack of well-constrained magnetization ages, and a persistent doubt that the recorded fields might be from transient impact-generated plasmas (Section 3.3) or magnetic contamination during sample handling rather than a lunar dynamo.

During the past decade, more detailed paleomagnetic studies have focused on samples with relatively high fidelity magnetic recording properties that are unbrecciated and at most weakly shocked (<5 GPa), are slowly cooled (so as to exclude putative impact-generated fields), and that have radiometrically defined and relatively precise NRM acquisition ages. Advances in ARM, SIRM, and double-heating paleointensity techniques and the practice of conducting paleomagnetic studies in conjunction with $^{40}Ar/^{39}Ar$ thermochronology have enabled confirmation that the lunar dynamo was active from at least ~4.25 Ga until it ceased sometime between ~1.92 and ~0.80 Ga (Garrick-Bethell et al. 2009, 2017; Cournède et al. 2012; Shea et al. 2012; Suavet et al. 2013; Tikoo et al. 2017, Mighani et al. 2020). These analyses, which are discussed further below, are summarized in Figure 3.

Several analyses of mare basalts confirmed the presence of strong surface fields, with a mean paleointensity of 78 μT, between at least ~3.85 and ~3.56 Ga (see review in Weiss and Tikoo 2014). Note that although the mean field during this period was apparently high, it is possible that more measurements from this period could reveal larger paleointensity variations, as the dataset is probably biased towards strong paleointensities that are easier to retrieve than lower ones. There are very few Apollo samples with NRM records older than ~3.9 Ga, and those that are this old are typically breccias produced by large, basin-forming events that exhibit shock deformation effects (and so have non-pristine magnetic records) and are slow-cooled (so are dominated by multidomain grains). Furthermore, the Apollo missions did not collect many rocks with ages between ~3.56 Ga and ~3.35 Ga, and surface volcanic activity on the Moon declined rapidly after this time. Therefore, these periods in lunar history are relatively unstudied.

Paleomagnetic measurements of mare basalts that formed at or after ~3.35 Ga indicate that the dynamo field intensity dropped by at least an order-of-magnitude somewhere between ~3.56 and ~3.2 Ga (Lawrence et al. 2008; Tikoo et al. 2014). However, sensitive paleointensity analyses of young lunar regolith breccias enabled by a controlled atmosphere oven have demonstrated the persistence of a weak dynamo after this time and identified when it ultimately ceased. In particular, an ~5 μT double heating paleointensity value was obtained from impact melt glass in a regolith breccia (Tikoo et al. 2017) that formed at 1.47 ± 0.45 Ga

(Mighani et al. 2020). This paleointensity result (as shown in Fig. 2c) passed a set of quality criteria (including checks for sample alteration) that are commonly adopted in terrestrial paleomagnetic studies (Shaar and Tauxe 2013). This measurement extends the lifetime of the lunar dynamo by at least ~1.5 billion years, and perhaps as much as ~2.5 billion years. A controlled-atmosphere double heating study of two young impact breccias with high fidelity magnetic recording properties (15465 and 15015) constrained lunar surface fields to <0.1 μT after 0.91 ± 0.11 Ga, indicating the cessation of the dynamo by this time (Mighani et al. 2020).

Many questions about the lunar paleointensity record persist. First, the short-term (thousands of years) variation of the field intensity, which could be used to constrain the velocity and geometry of flows in the core (e.g., Constable et al. 2016), is completely unknown. As an example, the much larger number of paleointensity measurements for Earth show that the Earth's field intensity has had excursions about the mean value of more than an order of magnitude over just the past 5 million years (Cromwell et al. 2015). Although differences in paleointensity values by a factor of 2–3 have been obtained for lunar rocks of similar age, whether this scatter is real or represents the loss of primary NRM in some rocks is unknown. It is also possible this scatter could represent real changes in field strength given that even high-fidelity terrestrial paleointensity records show similar dispersion (Selkin and Tauxe 2000). Second, there are as-yet no paleomagnetic measurements of the absolute direction of the lunar field (Schmitt et al. 2017), which would provide powerful constraints on the geometry and reversal rate of the dynamo and could be used to study the Moon's polar wander history (Section 3.4). Third, whether the lunar dynamo operated in a continuous or intermittent state prior to ceasing (Laneuville et al. 2014; Scheinberg et al. 2015) (Section 4.2) remains unknown given the sparse temporal sampling of lunar history as shown in Figure 3. Future efforts to answer these questions will provide critical constraints regarding the evolution of the lunar paleofield over time and the physical mechanisms that generated the dynamo.

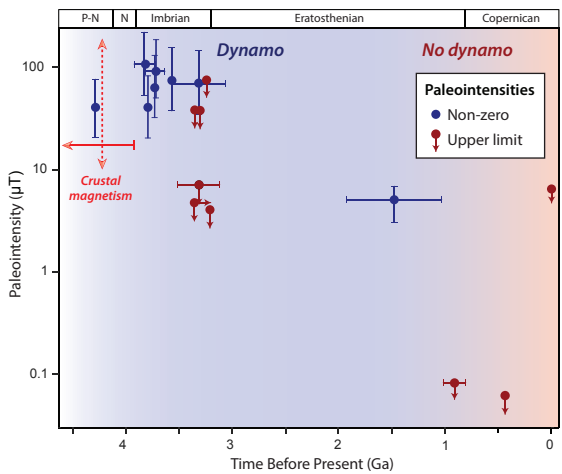

Figure 3. Paleointensity measurements of the lunar magnetic field using modern methods. Each point represents measurements of a single Apollo sample, **circles** represent actual paleointensities, **downward arrows** represent upper limits on paleointensity, and **right arrows** represent upper limits on age. Paleointensity uncertainties (including on upper limits) are typically a factor of two. The time range labeled "crustal magnetism" denotes the timing of strong dynamo fields from analyses of orbital crustal magnetic anomalies (see Section 3). The interiors of some basins of Nectarian (N) age exhibit clear strong remanence, and the ancient pre-Nectarian (P-N) aged highlands crust hosts weaker remanence (note that the paleointensity for the magnetizing field cannot be accurately inferred from orbial magnetic field data). The paleointensity dataset is from Lawrence et al. (2008), Cournède et al. (2012), Shea et al. (2012), Tikoo et al. (2012, 2014, 2017), Suavet et al. (2013), Buz et al. (2015), Garrick-Bethell et al. (2017), and Mighani et al. (2020). Sample paleointensities and ages are compiled in Table S22 of Mighani et al. (2020).

3. CRUSTAL MAGNETISM

Orbital measurements of the Moon's magnetic field show that the crust is magnetized. In this section, we summarize the orbital measurements that were made by the Lunar Prospector and Kaguya missions, discuss the global character of lunar magnetism, describe the magnetic signatures of impact basins, and summarize studies that have attempted to constrain the position of the magnetic pole from the inferred direction of crustal magnetization. For a discussion of how time-variable external magnetic fields generate induced magnetic fields that can be used to estimate the electrical conductivity profile of the Moon, we refer the reader to reviews by Sonett (1982), Hood (1986), Wieczorek et al. (2006), and Andrews-Hanna et al. (2023, this volume).

3.1. Magnetic field measurements and models

Measurements of the Moon's magnetic field were made during the Apollo missions from the low-altitude (~100 km) near-equatorial orbits of the Apollo 15 and 16 subsatellites, and from surface measurements at the Apollo 12, 14, 15, and 16 landing sites. The Apollo measurements were restricted to latitudes equatorward of 35° and global coverage was not obtained until 1998 when the Lunar Prospector mission obtained magnetometer and electron reflectometer measurements from a polar orbit. During the low-altitude phase of Lunar Prospector, measurements were made from an average altitude of about 30 km, with a range from 11 to 66 km. Magnetometer measurements were made later from the polar orbiting Kaguya mission (Tsunakawa et al. 2010) from altitudes of 9–80 km. One of the major difficulties in analyzing these measurements is that the fields originating from the Moon are weak at spacecraft altitudes, and that these measurements are contaminated by time-varying ambient fields with a typical amplitude of ~1–10 nT that are comparable to or larger than the signal from lunar fields. Plasma of solar wind and/or terrestrial origin can also compress and distort the lunar fields, so the best measurements are made in the lunar wake or geomagnetic tail lobe where plasma densities remain low.

Several studies have mapped lunar crustal magnetic fields either regionally or globally. In one technique (Richmond and Hood 2008; Hood 2011; Hood et al. 2013; Hood and Spudis 2016) the field measurements are extrapolated to a constant altitude and data are retained only where the external fields are slowly varying and of low amplitude. Purucker (2008) and Purucker and Nicholas (2010) alternatively used two different modeling techniques to remove the external fields in order to create global models from the Lunar Prospector magnetometer data. The final models were expressed using a spherical harmonic representation with a maximum spherical harmonic degree of 170, which resolves wavelengths as small as 64 km.

An alternative method for producing global and regional maps of the lunar crustal magnetic field was developed by Tsunakawa et al. (2010, 2014, 2015), who used an inverse boundary-value approach. This method combined both the Kaguya and Lunar Prospector magnetometer datasets and used only data collected between altitudes of 10 and 45 km within the lunar wake and geomagnetic tail. External fields were removed by a detrending procedure and the inversions provided global maps of the radial component of the surface field with a spatial resolution of about 6 km. The two horizontal components were then derived from the global model of the radial field, and the gridded data allowed construction of a spherical harmonic model with a maximum spherical harmonic degree of 450. More recently, Ravat et al. (2020) have performed global inversions using magnetic monopoles, combined with along-track magnetic field gradients and an L1-norm model regularization criterion. Their models have a similar spatial resolution as those of Tsunakawa et al. (2015), but have comparatively lower signal strengths beyond about spherical harmonic degree 200.

An independent estimate of the surface field strength can be obtained using the technique of electron reflectometry. This technique was discovered serendipitously in the Apollo era when electrons were unexpectedly observed coming from the direction of the Moon by an experiment on the Apollo-15 subsatellite (Anderson et al. 1975). These electrons represent electrons of external

origin that were reflected by electromagnetic fields near the lunar surface. Since the discovery of these reflected electrons, the Apollo 15 and 16 subsatellites (Anderson et al. 1975; Lin 1979; Lin et al. 1988), Lunar Prospector (Halekas et al. 2001; Mitchell et al. 2008), Kaguya (Harada et al. 2013), and ARTEMIS (Halekas et al. 2011) have used these measurements to probe the strength of lunar crustal magnetic fields at the surface of the Moon as well as electrostatic fields. Electron reflectometer techniques are sensitive to surface magnetic fields as weak as ~0.1 nT and can resolve crustal magnetization with scale sizes as small as ~5–10 km (Lin 1979; Halekas et al. 2010). This technique provides more sensitivity to weak and incoherent fields present at the surface than do the orbital magnetometer measurements whose intrinsic spatial resolution is approximately equal to the spacecraft altitude. Unlike the magnetometer measurements, electron reflectometer studies are sensitive only to the total field strength and not the direction of the field.

3.2. Global properties of crustal magnetism

The total magnetic field strength of the Tsunakawa et al. (2015) model is presented in Figure 4 at an altitude of 30 km above the mean planetary radius. In the upper row, the field strength is plotted using a linear scale for both the near and farside hemispheres of the Moon, and in the lower row the field strengths are plotted using a logarithmic scale. The crustal field strengths are lower than about 1–2 nT over the vast majority of the Moon, and when the field strength is plotted using a logarithmic scale, two prominent regions with exceedingly low (<0.1 nT) intensities are observed. One of these low-intensity regions is on the nearside hemisphere and encompasses Mare Imbrium, the surrounding highlands, and a portion of Oceanus Procellarum. The other region is about a quarter of the size of the nearside anomaly and is located entirely in the northern farside highlands. Both of these low-field regions are visible in the magnetic field strength maps derived from the electron reflectometer experiment (Halekas et al. 2001; Mitchell et al. 2008). The largest concentration of contiguous mare basalts on the Moon is located within Oceanus Procellarum and Mare Imbrium, the majority of which are associated with low field strengths (Halekas et al. 2001). Outside of the nearside magnetic low, however, the maria are not substantially different in field strength than the surrounding highlands.

One interpretation for the nearside magnetic low is that the shock wave generated by the Imbrium impact event could have partially demagnetized the surrounding crust (Halekas et al. 2003; Mitchell et al. 2008). However, even though the Imbrium impact basin is one of the largest basins on the Moon, the size of the anomaly and its uniformly weak nature makes it unlike the signatures of other comparably sized basins. Alternatively, as shown in Figure 4, Wieczorek (2018) noted that the nearside magnetic low lies entirely within the confines of the Procellarum KREEP (an acronym for potassium rare-earth elements and phosphorous) Terrane, which is a region of the Moon that is enriched in heat-producing elements and that had higher than average temperatures over prolonged periods of time (Jolliff et al. 2000; Wieczorek and Phillips 2000). Thermal evolution models show that it could take more than a billion years for the entire crust of this region to cool below the Curie temperature of metallic iron (Laneuville et al. 2018). If the dynamo field turned off (or weakened) before this happened, the deeper portion of the crust could have escaped becoming magnetized. Neither of the impact demagnetization nor KREEP hypotheses can account for the origin of the magnetic low on the farside hemisphere, as this region is not associated with an impact basin, enhanced abundances of heat producing elements, or evidence of magmatic activity.

Several isolated anomalies with strong field strengths are located on both hemispheres of the Moon and a large concentration of extended anomalies is located in the southern farside highlands. Though a few anomalies with moderate to strong field strengths are found in the interiors of impact basins or near their antipodes (Section 3.3), most impact basins are not associated with strong fields. Some basin ejecta deposits do have statistically higher than average field strengths, such as the Cayley formation that is interpreted as ejecta from the Imbrium basin. However, other ejecta from the same basin, such as the Fra Mauro formation,

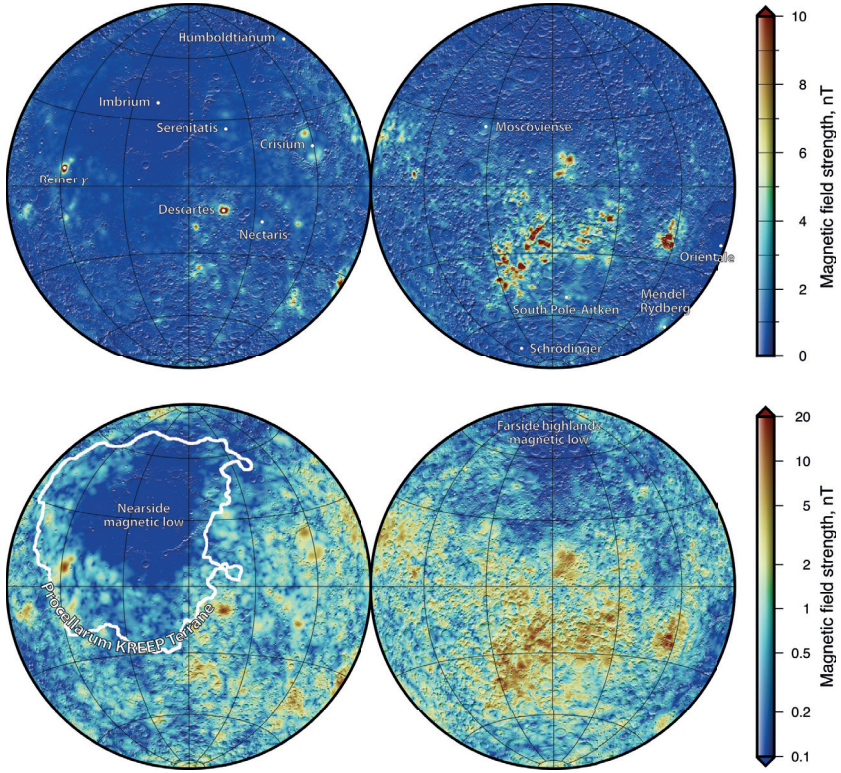

Figure 4. Total magnetic field strength of the Moon at 30 km altitude plotted using a linear (**top**) and logarithmic (**bottom**) color scale. The field strength maps are presented in Lambert azimuthal equal-area projections centered over the nearside (**left**) and farside (**right**) hemispheres and are overlain by a shaded relief map derived from the Lunar Orbiter Laser Altimeter (Smith et al. 2010). Grid lines are spaced every 30° in latitude and longitude. Magnetic field data are from Tsunakawa et al. (2015), which includes both Lunar Prospector and Kaguya measurements. The Procellarum KREEP Terrane is defined by the 4 ppm contour of thorium (see Jolliff et al. 2000).

have average field strengths (Halekas et al. 2001). The isolated Descartes magnetic anomaly that is close to the Apollo 16 landing site is in a region covered by ejecta from the Imbrium impact basin, but the field strengths associated with most Imbrium ejecta are substantially weaker.

A few strong anomalies are suggestive of an origin related to magmatic processes. Purucker et al. (2012) highlighted a set of strong linear magnetic features in the northwestern portion of the South Pole–Aitken basin. These have lengths of about 1000 km and, given that they do not have any surface expression, they were interpreted as a subsurface swarm of magnetized magmatic dikes. These features are unrelated to the linear dike-like features seen in the GRAIL gravity data (Andrews-Hanna et al. 2013). Another possible correlation with magmatic processes is the prominent Reiner-γ magnetic anomaly in Oceanus Procellarum. This anomaly is only a few hundred km away from the center of the Marius Hills volcanic rise, which is a region that experienced prolonged and intense volcanic activity (Spudis et al. 2013). Inversions for the strength of magnetization over this region show the existence of a linear magnetization anomaly that connects the Reiner-γ magnetic anomaly to the center of Marius Hills (Oliveira and Wieczorek 2017). This linear anomaly could conceivably represent a magmatic dike that cooled in the presence of a dynamo field.

Most magnetic anomalies have no clear association with either surface geomorphology or lunar geologic processes. Constraints on the origin of these anomalies could thus be obtained if it were known at which depths the magnetic sources were located. For example, magnetized impact ejecta and mare basalts would be expected to be located close to the surface, whereas magmatic intrusions and primordial crustal magnetization would be located at greater depths. Wieczorek (2018) made use of a statistical model of magnetization with a localized spectral analysis approach to estimate the depth range of crustal magnetism. Depths to the top of the magnetized zone were found to vary from the surface to about 25 km. Although some of the crustal magnetization could be associated with near-surface impact deposits, the majority of crustal magnetization is located deeper than 10 km below the surface. It is unlikely that this deep magnetization is a result of intrusive magmatism given that most regions in the highlands show no association with volcanic products. The simplest explanation is that the deep magnetization is a result of primordial magma ocean cumulates that were magnetized as they cooled in an internally generated dynamo field. Thermal evolution models predict that the highland crust outside of the Procellarum KREEP Terrane would have cooled below the Curie temperature of metallic iron about 100 million years after crust formation (Laneuville et al. 2018), implying that an internal dynamo must have existed during at least part of this time period.

The depth and origin of crustal magnetization can also be constrained using the lunar gravity field (Gong and Wieczorek 2020). Although most magnetic anomalies have no clear association with gravity anomalies, about 3–10% of the Moon's surface area does possess local correlations between free-air gravity and magnetic field strength that are statistically higher than would be expected by chance. Importantly, only those regions that have positive correlations are statistically significant. As the free-air gravity is largely a result of surface topography, and most surface relief is due to impact cratering, this implies that the statistically significant positive correlations are caused largely by magnetized materials that were added to the surface of the Moon, as might be expected for ejecta from impact basins. Consistent with this hypothesis, these regions have shallower than average depths of magnetization as calculated by Wieczorek (2018). A smaller portion of the lunar surface also shows statistically significant positive correlations with the Bouguer gravity. The Bouguer gravity reflects subsurface density anomalies, implying that the magnetization of the regions is associated with denser than average crustal materials, such as might be expected for magmatic intrusions.

Many of the strongest lunar magnetic anomalies are associated with swirl-like albedo markings on the surface (e.g., Hood and Williams 1989; Blewett et al. 2011; Denevi et al. 2016). It has been proposed that these curious surficial bright and dark optical markings could be the result of local variations in space weathering due to magnetic deflection of solar wind (Hood and Schubert 1980; Bamford et al. 2016; Deca et al. 2018, 2020) or magnetic/electrostatic sorting of fine-grained materials (Garrick-Bethell et al. 2011). A relevant property of both models is that the morphology of the swirls should be directly related to the near-surface magnetic field structure (Hemingway and Garrick-Bethell 2012). The characteristic bright-to-dark transition length scale of swirls is typically about 1–5 km, and this requires the magnetic field direction to vary over similar length scales. In one model (Hemingway and Tikoo 2018), the magnetic source bodies need to be both shallow (< 1–5 km deep) and narrow. These restrictions on the geometry and volume of the magnetic sources implies that the source magnetization must exceed ~0.5 A m^{-1} and is likely less than 6 A m^{-1} (see also Nicholas et al. 2007). In another model, edge effects from a shallow but considerably wider (~13 km) magnetized disk give rise to a similar magnetic field morphology, with predicted magnetizations up to ~70 A m^{-1} (Garrick-Bethell and Kelley 2019). Whereas basalts on Earth typically have magnetizations of several A m^{-1}, and crustal rocks on Mars can reach several 10s–100s of A m^{-1} (e.g., Whaler and Purucker 2005; Schmidt et al. 2007), lunar mare basalts typically have magnetizations < 0.01 A m^{-1}, indicating that these lunar crustal source bodies are either unusually rich in metallic iron or that they were magnetized by a field much stronger than what has been inferred for the lunar dynamo.

3.3. Magnetic signature of impact basins

Impact cratering is the primary geological process that has shaped the surface of the Moon, and this process has been postulated to account for several aspects of lunar magnetism. Impact events heat and melt portions of the crust, allowing the rocks to acquire a thermoremanent magnetization if a field is present, while impact-generated shock waves can demagnetize the crust. Moreover, impacts can also deliver magnetic materials to the Moon and potentially generate transient magnetic fields.

Initial mapping of impact basins by the Lunar Prospector electron reflectometer showed that a basin's magnetic signature correlated with its age (Halekas et al. 2003). The youngest Imbrian-aged basins (3.7–3.9 Ga; Schrödinger, Orientale and Imbrium) have field strengths in their interiors that are weaker than their surroundings, whereas many of the older Nectarian aged basins (from 3.9 to ~4.1 Ga) possess central magnetic highs. The pre-Nectarian basins are more variable with the oldest not having any distinguishing magnetic signature. These results were later confirmed by Lunar Prospector and Kaguya magnetometer data, where central magnetic highs were mapped in the Nectarian-aged basins of Humboldtianum, Nectaris, Crisium, Mendel–Rydberg, Moscoviense, and Serenitatis (Hood 2011; Le Bars et al. 2011). With the exception of Crisium, the central field strengths are relatively weak with amplitudes of only a few nT at 30 km altitude. The simplest interpretation of these observations is that the internal dynamo was much weaker during the Imbrium period than it was during the Nectarian (Hood and Spudis 2016). This conclusion, however, contrasts with paleomagnetic analyses that indicate Earth-like field strengths extend well into the Imbrian period (Section 2 and Fig. 3).

Inversions for the strength and distribution of magnetization in the Nectarian-aged basins show that the magnetic materials are located almost entirely within the inner depression of the basin (Oliveira et al. 2017). The inner depression is a structural feature that lies just interior to the peak ring and that is interpreted to have formed by thermal contraction of a thick impact melt sheet (Vaughan et al. 2013). It would take less than 1 million years to cool a 5 km thick melt sheet below the blocking temperature of metallic iron (Le Bars et al. 2011), implying that the melt sheet could have acquired a substantial TRM only if a magnetizing field existed that was stable in direction over this same time interval. The implied magnetizations are consistent with small quantities of metallic iron in the melt sheet, from 0.1 to 0.45 wt% (Oliveira et al. 2017). Given that most indigenous lunar rocks have considerably lower abundances of iron metal, a plausible interpretation is that this metal was derived from the projectiles that formed these basins. The mafic impact-melt breccias derived from the Imbrium impact basin contain up to 2 wt% metal of meteoritic origin (Korotev 2000), and comparable amounts of projectile contamination can be found in terrestrial impact melts (Tagle and Hecht 2006; Tagle et al. 2009).

Electron reflectometer data show that many impact craters with diameters from about 50 to 400 km are associated with a demagnetization signature (Halekas et al. 2002). The field strengths are generally about 20% lower within ~2–4 crater radii than in the surroundings, and this signature is approximately independent of the setting of the crater, the crater size, and the crater age. Since the demagnetization signature extends far beyond the crater rim, impact-generated shock waves are likely responsible for demagnetizing the crust, and not thermal effects associated with crater formation. The fact that some pre-Nectarian craters possess a demagnetization signature implies that the pre-Nectarian crust must have been previously magnetized.

The largest concentration of strong magnetic anomalies is located in the central farside highlands of the Moon. One model that was proposed to account for the origin of the high field strengths there was motivated by the observation that these regions are approximately antipodal to three young large impact basins (see Fig. 5): Imbrium, Serenitatis, and Crisium (Lin et al. 1988; Hood and Williams 1989; Hood 1995; Mitchell et al. 2008). The young Imbrian-aged Orientale

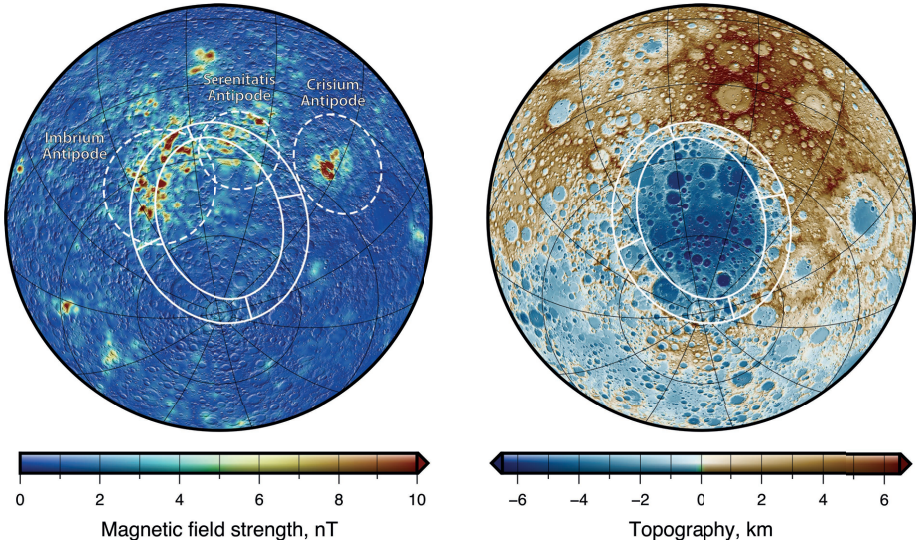

Figure 5. Total magnetic field strength of the Moon (**left**) and surface elevations (**right**) centered over the farside South Pole–Aitken impact basin. The field strengths are from the model of Tsunakawa et al. (2015) and are plotted at 30 km altitude, and the surface topography is from the Lunar Orbiter Laser Altimeter (Smith et al. 2010). **Ellipses** elongated in the north–south direction denote the inner floor and outer structural rim of the basin (Garrick-Bethell and Zuber 2009), and the connecting lines join the respective semiminor and semimajor axes. **Dotted circles** denote the antipodes of the Imbrium, Serenitatis and Crisium basins, where the circle size corresponds to the basin size from Neumann et al. (2015). All images show half of the lunar surface and are displayed in a Lambert azimuthal equal-area projection overlain by a shaded relief map derived from the surface topography. Grid lines are spaced every 30° in latitude and longitude.

and Schrödinger basins are also associated with magnetic anomalies close to their antipodes (Hood et al. 2013). It was hypothesized that an impact-generated vapor cloud, which would be partially ionized due to high temperatures, would expand and converge at the antipode of the basin (Hood and Vickery 1984; Hood and Huang 1991; Hood and Artemieva 2008). As the vapor cloud converged, it would compress and amplify the strength of the ambient field, which could be of either solar or lunar origin. The near-simultaneous convergence of ejecta (Wieczorek and Zuber 2001; Hood and Artemieva 2008) and/or seismic waves (Schultz and Gault 1975; Hughes et al. 1977; Watts et al. 1991) would then contribute to magnetizing the local materials. (Alternatively, the basin ejecta deposited near the antipode could be the source of the magnetic materials that were subsequently magnetized.) The initial studies consisted of simulations of vapor generation by the impact and its hydrodynamic evolution over time, and the models predicted that strong fields (several μT) could be generated that could last for about one day (Hood 1987).

The above studies, however, did not model the magnetic field evolution after the impact, which is coupled to the motion of the conducting gas around the Moon and the induction currents inside the resistive lunar interior. Instead, the magnitude of the compressed magnetic field was evaluated from conservation of magnetic energy, and the duration of the compressed fields was estimated from thermal and magnetic energy balance at the antipode. Furthermore, these models did not take into account either the loss of magnetic energy by diffusion inside of the Moon nor the escape of conducting impact vapor from the lunar gravitational field. Oran et al. (2020) revisited the impact-amplified field hypothesis by coupling an impact shock-physics numerical code to a state-of-the-art magnetohydrodynamics (MHD) code. They performed three-dimensional simulations where the Moon initially contained an induced field of 30 nT, which is a likely upper limit for an ancient solar wind field. The simulations included the expansion

of the vapor cloud and the inductive response of the Moon using a realistic resistivity profile. Their results showed that loss of magnetic energy due to ohmic dissipation, mostly in the lunar crust and upper mantle, is a major limiting factor of the maximal field enhancement that can be achieved. In fact, they showed that the crustal resistivity is capable of removing the entirety of the initial induced field inside the crust and mantle within seconds to minutes after the vapor cloud engulfs the Moon. Moreover, the conducting vapor effectively separates the Moon from the solar wind field and no new magnetic energy is added to the system. While a compression of the initial induced field occurs at the cloud periphery as it pushes away the solar wind plasma, these enhancements are at least 2–3 orders of magnitude too small and are too short-lived to explain basin antipodal magnetization under any scenario explored. These results and the prohibitive effects of ohmic dissipation refute the possibility that an externally induced field by itself can be amplified and explain lunar magnetization.

An alternative origin for the farside magnetic anomalies was proposed by Wieczorek et al. (2012), who noted that the strongest anomalies were located on the northern rim of the South Pole–Aitken basin (Fig. 5). This basin was proposed to have formed under oblique conditions, with the projectile traveling from the south to north (Garrick-Bethell and Zuber 2009) and hydrocode simulations show that under moderately oblique conditions, significant quantities of projectile materials could be deposited on the northern rim, precisely where the magnetic anomalies are found. The projectile materials could be derived either from an undifferentiated chondrite or from the core of a differentiated planetesimal, both of which contain considerably more metallic iron than indigenous lunar crustal rocks. The simulations predict integrated thickness of a few hundred meters to a few km of projectile materials on the rim of the South Pole–Aitken basin. If these were magnetized in the presence of a global field with Earth-like strengths, the predicted strength of the magnetic anomalies would be comparable to the observations.

3.4. Magnetic paleopoles

For many dynamos in our solar system, the field is predominantly dipolar, and the dipole axis is nearly aligned with the body's spin axis. Earth, Mercury, Ganymede, Jupiter, Saturn, and the Sun all have dipole axes that are inclined by less than about 10° with respect to their spin axes (Christensen 2019). Furthermore, the mean field of the Earth over the last ~10,000 years has been nearly perfectly aligned with the spin axis (Cromwell et al. 2015). In such cases, the field geometry on the surface changes predictably with latitude. Hence, if the original geographic location and orientation of a rock mass were known, one might be able to use measurements of its magnetization direction to infer the geographic location of the body's magnetic pole at the time of remanence acquisition, and by consequence the spin axis.

When mass is redistributed within a body (such as through impact cratering or mantle convection), the solid portion of the planet can reorient with respect to the spin axis by the process of true polar wander. Based on analyses of the global shape of the Moon, as well as the distribution of hydrogen near the poles, up to 40° of true polar wander could have occurred over lunar history (Garrick-Bethell et al. 2014; Keane and Matsuyama 2014; Siegler et al. 2016). The temporal evolution of true polar wander could perhaps be deduced from the magnetization directions of lunar rocks if their ages were known. Nevertheless, there are several complications that could hinder such an attempt: it is unknown if the lunar dynamo field was primarily dipolar or multipolar (Christensen and Aubert 2006; Soderlund et al. 2012; Oruba and Dormy 2014), it is unknown if the dipolar component of the field was always aligned with the spin axis (Takahashi and Tsunakawa 2009), and it is possible that the rotation axes of the solid mantle and core could have differed by up to ~45° when the Earth–Moon separation was less than 40 Earth radii (Ćuk et al. 2019). An important consequence of the dynamo field geometry is that it may have controlled the accumulation of volatiles at the lunar poles (Garrick-Bethell et al. 2019).

One way that the geometry of the lunar magnetic field could be studied would be to analyze the direction of magnetization in oriented samples of lunar bedrock. Unfortunately, none of the Apollo samples were unambiguously collected from in situ bedrock. In certain circumstances, it is possible to infer the paleo-horizontal plane by using proxies such as magnetic anisotropy. The magnetic foliation plane was used by Cournède et al. (2012) to determine the inclination of the magnetization direction for seven different rocks collected at three different Apollo sites. Assuming a dipolar field, the inferred paleolatitudes were found to differ from the actual latitudes of where the samples were collected by less than 17°, consistent with the dipole axis being approximately oriented with the present rotation axis when the rocks were magnetized.

A number of studies have been performed over the last 40 years that have attempted to constrain the location of the Moon's past magnetic poles using orbital magnetometer data. Since these studies explicitly assume an ancient dipolar field, these magnetic poles are often referred to as paleopoles or virtual geomagnetic poles. Given that dynamos may exhibit polarity reversals, we summarize these results by plotting both the north and south geomagnetic paleopoles together on a single hemisphere in Figure 6. As is seen, when treated together, there is little agreement in the paleopole locations. Nonetheless, some studies have purported to find a clustering of paleopoles in specific regions that can be used to trace the temporal evolution of lunar true polar wander. Work in this category begins with Runcorn (1982, 1983) who found three clusters of paleopoles in three different epochs with evidence for polarity reversals. Later, Takahashi et al. (2014) reported two paleopole clusters, one coincident with the Moon's current spin axis, and another interpreted to represent ~45–60° of true polar wander. Arkani-Hamed and Boutin (2014, 2017) studied isolated anomalies and those from demagnetized impact craters, and similarly found evidence for clustering in both cases. Finally, Tsunakawa et al. (2015) examined four anomalies at impact crater centers, and compared the inferred paleopoles with previously reported clusters. However, none of the major clusters reported above show strong overlap.

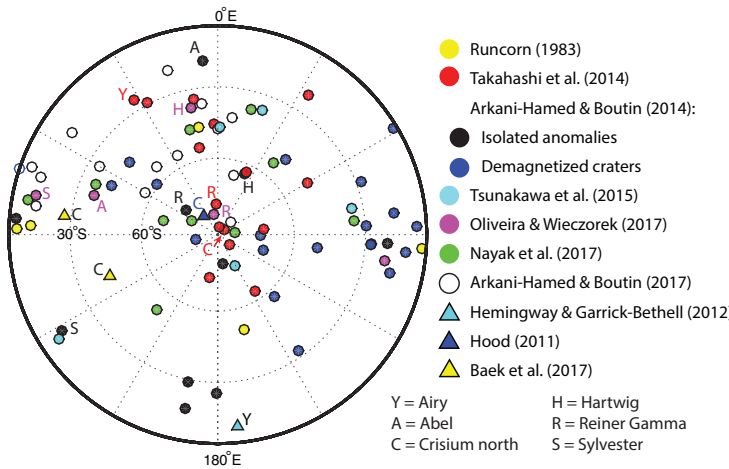

Figure 6. Equal area projection of nearly all published lunar magnetic paleopoles, in the southern hemisphere of the Moon. All northern hemisphere paleopoles are reversed into the southern hemisphere under the assumption that polarity reversals may take place. Scatter is larger if all paleopoles are not reversed. Letters indicate magnetic anomalies that are repeated across different studies. Paleopoles from Oliveira and Wieczorek (2017) are for their five best-fitted anomalies. Paleopoles from Takahashi et al. (2014) are for anomalies shown in their Figure 3, with values from their Tables S1 and S2, with repeated anomalies averaged together. Paleopoles from isolated anomalies in Arkani-Hamed and Boutin (2014) are the means of values in their Table 2. Paleopoles from Runcorn (1983) are the means of the first three clusters in his Table 1. Error ellipses, if reported, have been omitted for clarity.

In contrast, other studies find no obvious clustering in the paleopole locations, and no obvious relationship between paleopoles and true polar wander. Hood (1981) found widely scattered paleopoles. Nayak et al. (2017) examined magnetic anomalies in the South Pole–Aitken basin and concluded that there was no obvious clustering. They instead argued that the Moon should have experienced only modest amounts of true polar wander, and suggested that the dynamo dipole axis may not have been spin-axis aligned when the magnetic anomalies formed. Similar conclusions were reached by Oliveira and Wieczorek (2017), where the best constrained paleopoles were found to span all latitudes. Their best-determined paleopoles appeared to avoid the nearside maria and a possible distribution on a great circle along 90° W and 90° E longitude was noted. They suggested that this great-circle alignment could be explained by a rotating dipole axis, possibly controlled by a dynamo with a nearside–farside asymmetry in heat flow at the core–mantle boundary (Takahashi and Tsunakawa 2009).

When all published paleopoles are examined together, there is little coherence. If all studies were treated equally, one would be justified to conclude one or more of the following: (1) the magnetizing field was not predominantly dipolar, (2) the dipole axis was not predominantly oriented in a single direction, (3) the magnetizing field was highly variable in direction and time, or (4) the crustal magnetic anomalies are not unidirectionally magnetized. There are several potential explanations for the lack of consensus on the meaning of the lunar magnetic paleopole results. Perhaps most importantly, there is no agreed upon method for choosing suitable magnetic anomalies for analysis, and several different approaches have been used to estimate magnetization directions and paleopole uncertainties (see Vervelidou et al. 2017; Maxwell and Garrick-Bethell 2020). As an example, Oliveira and Wieczorek (2017) used a method developed by Parker (1991) that assumes unidirectional magnetization in the crust, but makes no other assumptions about the source geometry. Other studies have made more restrictive assumptions about the source geometry, including the use of dipoles, prisms, and disks. Another key problem is that little is known about the formation of the investigated magnetic anomalies. Thus, grouping anomalies by surface age or geologic unit can be problematic since the anomalies rarely show any clear genetic relationship with surface geology. Even anomalies within well-dated craters may have formed long after the crater by intrusive volcanism.

4. DYNAMO GENERATION

Paleomagnetic analyses of Apollo samples and measurements of the Moon's crustal magnetic field both imply the existence of a long-lived magnetic field that arose as early as 100 million years after crust formation and persisted (at least intermittently) until as late as ~1 Ga. Given this duration, the most plausible origin of these fields is from an internal dynamo that converts kinetic energy to magnetic energy via the induction process. Since the Moon is known to have a small partially molten metallic core whose radius is ~200–380 km (e.g., Williams et al. 2014), dynamo activity is often to assume to have occurred in the core. Nevertheless, it has also been postulated that a molten silicate basal magma ocean might also have generated a dynamo. In this section, we review the different energy sources and models that have been proposed to power magnetic field generation. These include dynamos powered by thermal convection, core crystallization, precession of the solid mantle and/or solid inner core, and inertial instabilities via changes in the rotation rate following basin-forming impact events.

4.1. Thermal dynamos

Magnetic field generation requires motion of an electrically conducting liquid. One possibility for driving fluid motions is a sufficiently large superadiabatic temperature difference between the solid mantle and the fluid dynamo region, which gives rise to thermal convection in the fluid. This so-called thermal dynamo occurs if the heat flux q_d at the top of the fluid exceeds that conducted along the adiabat q_{ad}. This serves as a necessary but not sufficient criterion for the existence of thermally driven convection and is given by

$$q_{\mathrm{d}} > q_{\mathrm{ad}} = k_{\mathrm{d}} \left.\frac{dT}{dr}\right|_{\mathrm{ad}} = k_{\mathrm{d}} \alpha_{\mathrm{d}} g_{\mathrm{d}} \frac{T}{C_p} \quad (5)$$

where k_d is the thermal conductivity of the fluid dynamo region, $dT/dr|_{ad}$ is the adiabatic temperature gradient of the fluid, α_{d} is the thermal expansivity of the fluid, C_p is the heat capacity at constant pressure of the fluid, and g_{d} and T are the gravitational acceleration and temperature at the interface of the dynamo region and overlying solid mantle. If $q_{\mathrm{d}} < q_{\mathrm{ad}}$, the fluid layer will be stably stratified and dynamo action by thermal convection will not be possible. Assuming that dynamo activity occurs in the metallic core, the critical heat flux is estimated to vary between 2 and 10 mW m^{-2} (Stegman et al. 2003; Zhang et al. 2013; Evans et al. 2014; Laneuville et al. 2014; Silber et al. 2018), where the most uncertain parameters are the thermal conductivity and thermal expansivity of the fluid core. For a 330 km radius core, the total amount of energy removed from the core per unit time would be 3–14 GW.

In addition to the heat flux criteria, dynamo activity will occur only if the magnetic Reynolds number, R_{m}, is greater than a critical value that is about 40 (Christensen and Aubert 2006). The magnetic Reynolds number characterizes the importance of magnetic advection in comparison to magnetic diffusion and is defined as the product $\mu_0 \sigma U D$, where μ_0 is the magnetic constant, σ is the electrical conductivity, U is the flow speed, and D is the thickness of the convecting region. This criterion is satisfied when convection occurs in a metallic fluid with high electrical conductivity but is difficult to achieve for molten silicates.

Most thermal and magnetic field evolution models have considered a thermally driven core dynamo during the early evolution of the Moon (Konrad and Spohn 1997; Spohn et al. 2001; Laneuville et al. 2014). These models show that if the core was superheated by a few hundred degrees with respect to the mantle, such a dynamo would have been active since core formation and may have lasted a maximum of a few hundred Myr (until no longer than 4 Ga). A thermal core dynamo could perhaps account for the magnetic anomalies associated with impact basins and the ancient crust, but cannot explain the existence of a global field as required by paleomagnetic analysis of young (<4 Ga) samples (see Figs. 3 and 7).

Thermal dynamo models have subsequently been modified to consider the potential consequences of a crystallizing lunar magma ocean (Stegman et al. 2003; Zhang et al. 2013; Scheinberg et al. 2015). A dense ilmenite and pyroxene cumulate layer with high abundances of KREEP is predicted to form between the crust and mantle at the terminal stages of magma ocean crystallization, and some models predict that these materials would sink all the way to the core–mantle boundary (e.g., Parmentier et al. 2002). In this model, the dense, KREEP-rich layer thermally insulates the core, such that the core heat flow is initially below the limit for convection, and dynamo action is delayed (Fig. 7). Eventually, because of heating by the radiogenic elements, the ilmenite-rich layer becomes buoyant and convection lifts it from the core–mantle boundary. With removal of the thermal blanket, the core begins to convect vigorously. Nevertheless, recent models by Zhang et al. (2017) show that the ilmenite-rich cumulates could actually remain stable at the core–mantle boundary and not rise towards the surface due to their weaker rheology and more efficient heat transfer to the overlying mantle.

The majority of the thermal evolution models discussed above have considered a dry mantle. Recent studies, however, suggest that water is more abundant in the lunar interior than previously thought (e.g., Saal et al. 2008; Grimm 2013; Klima et al. 2013; McCubbin et al. 2015) and its distribution in the interior is possibly inhomogeneous as a consequence of magma ocean solidification (Elkins-Tanton and Grove 2011; McCubbin et al. 2011). This observation may have profound implications for the thermochemical evolution of the Moon because water, even in small concentrations, is known to have a strong effect on mantle rheology, with a viscosity reduction of more than a factor of 100 between water-saturated and completely dry material.

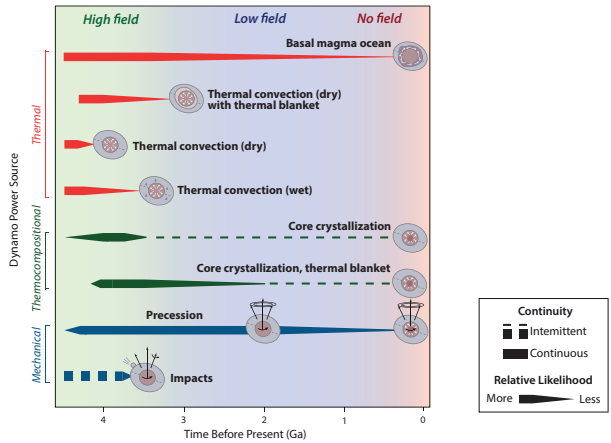

Figure 7. Timing of proposed dynamo mechanisms in relation to the temporal evolution of the surface field strength. From top to bottom are plotted thermal dynamos, thermo-chemical convection dynamos driven by core crystallization, and mechanical dynamos (precession and impact induced changes in rotation). For each mechanism, tapering at the ends of the interval denotes uncertainties in either the start or stop time of dynamo activity. **Dashed lines** indicate that dynamo activity may potentially be episodic, or reactivated at a later time. The transition from the high-field to low-field epochs occurs sometime between 3.56 and 3.19 Ga, and the dynamo ceases sometime between 1.9 and 0.8 Ga.

Evans et al. (2014) showed that a long-standing thermal dynamo of up to 2 billion years is possible (Fig. 7) if the lower mantle rheology is weakened by water and the core is assumed to have a low thermal conductivity of 25 W m^{-1} K^{-1}, corresponding to an adiabatic heat flux of 2.4 mW m^{-2}. However, if an upper bound on the adiabatic heat flux of 10 mW m^{-2} is instead considered, the duration of this thermal dynamo would be reduced to about 500 million years.

To estimate the magnetic field strength of a lunar dynamo, scaling laws that relate magnetic energy to convective power available for the dynamo (assumed to balance ohmic dissipation) are most frequently used (see Christensen 2010 for a review). These scaling laws also require assumptions about the (unknown) dominant force balance in the dynamo region. The mixing length formulation is often employed (cf. alternative Coriolis–inertia–Archimedean and magneto–Archimedean–Coriolis force balances), such that the surface field intensity is given by an equation of the form

$$B_{\text{surf}} = f \mu_0^{1/2} \rho_{\text{d}}^{1/6} \left(\phi D \right)^{1/3} \left(\frac{R_{\text{d}}}{R_{\text{p}}} \right)^3 \tag{6}$$

where f is an efficiency prefactor that includes the partitioning of energy into the external dipole component, ρ_{d} is the density of the dynamo region, ϕ is the volumetric ohmic dissipation rate, D is the thickness of the convecting region, R_{d} is the radius of the dynamo region, and R_{p} is the planetary radius. The final cubic term accounts for the geometric decrease of the dipole component from the top of the dynamo region to the Moon's surface. For a thermally driven dynamo, the volumetric ohmic dissipation rate is given by the power associated with the heat flux out of the core minus the power from the heat that can be conducted along the adiabat.

The strength of the surface magnetic field obtained by a thermal dynamo in the core has been estimated to be of the order of 0.1–2 μT (e.g., Evans et al. 2014, 2017; Laneuville et al. 2014). This range is ~5–100 times lower than the paleomagnetic field strengths for times younger than 3.56 Ga (< 10 μT), and is about 35–700 times lower than the strong fields before this time (~70 μT). Field strengths stronger than ~1 μT are unlikely for thermal dynamos

because B_{surf} scales with $\varphi^{1/3}$. An order of magnitude increase in the field strength requires a three order of magnitude increase in available power.

One of the reasons strong magnetic fields are difficult to achieve on the Moon's surface is the R_p^{-3} decay of the dipole field strength from the core–mantle-boundary to the surface. This geometric effect implies a reduction of a factor of at least 100, which is significantly less than the factor of about 7 that occurs for Earth. For this reason, the hypothesis of a magnetic field generated closer to the surface, namely in a silicate basal magma ocean that is above the metallic core, has been studied by Scheinberg et al. (2018). They show that a dynamo could potentially be generated in such a basal magma ocean between about 4.2 and 1.6 Ga for their nominal case, but with durations that could range from ~0 to the entirety of lunar history given the uncertainty of the input parameters (Fig. 7). Nominal field intensities reach 4–14 μT, and could potentially be as high as 40 μT in the most optimistic model. The corresponding minimum electrical conductivities necessary to sustain such a dynamo were reported to range between 3000 and 30,000 S m^{-1} for a critical R_m of 10, but these would be even larger for the larger values of R_m reported in the literature (cf. Christensen and Aubert 2006). In comparison, Pommier et al. (2015) conducted electrical conductivity experiments for olivine (Fo_{77}) at conditions relevant for the lower lunar mantle and found melt conductivities of 78 ± 8 S m^{-1}. High abundances of FeO, TiO_2 and/or water in the melt may increase the electric conductivity, but experimental data are lacking to test whether an increase by a factor of ~100 or more is feasible.

4.2 Core crystallization

It is possible to have fluid motions that can power a dynamo even when the heat escaping the core is less than the heat conducted along the core adiabat. As the core temperature decreases, solid iron can begin to crystallize, which liberates light elements and releases latent heat. Core crystallization can power a dynamo when it occurs at the boundary of the inner core, where the liberated light elements cause the fluid to rise, or at the core–mantle boundary, where dense iron crystals sink in the fluid (Williams 2009). Key parameters for core crystallization models include the bulk abundance and type of light alloying elements in the core, the core–mantle boundary temperature, and the rate of core crystallization.

The temperature evolution of the core is usually predicted by a global thermal evolution model that couples the mantle to the core. These models should match observational constraints when they exist, such as the duration and distribution of mare volcanism, solid inner core size, and core–mantle boundary temperature. Inversions of lunar geophysical data by Khan et al. (2014) suggest that the present-day core–mantle boundary temperature is about 1900–2100 K. However, by considering the effect of water on electrical conductivity and seismic attenuation, Karato (2013) found that the core–mantle boundary temperature could be as low as 1500 K. The present-day inner core size is poorly constrained based on geophysical measurements, with estimates ranging from 0 to 280 km (Garcia et al. 2011; Weber et al. 2011; Matsuyama et al. 2016). Since at least part of the lunar core is still liquid today (Williams et al. 2001), the inner core must be smaller than the total core radius, which is estimated to lie between 200 and 400 km (Shimizu et al. 2013; Williams et al. 2014; Matsuyama et al. 2016).

The abundance of light alloying elements in the core can be estimated from analyses that make use of geophysical constraints such as core density, temperature, and seismic velocity. Estimates of the bulk sulfur content based on analyses of seismic data range from about 3 wt% (Weber et al. 2011) to 10 wt% (Garcia et al. 2011). Experiments by Antonangeli et al. (2015) have since provided updated equations of state for the Fe-S system and better estimates of seismic velocities of core materials. When combined with the seismic model of Weber et al. (2011) (with a core radius of 330 km), these results imply bulk core sulfur contents of 3–6 wt% and an inner core radius of 245–250 km.

The bulk core composition can also be estimated using the depletion of siderophile elements in the mantle along with a model of metal–silicate equilibration. Rai and van Westrenen (2014) found that a lunar core with 6 wt% sulfur that equilibrated at core–mantle boundary pressures (~4–5 GPa) was consistent with the observed siderophile elements pattern. Later, Steenstra et al. (2016) demonstrated that if equilibration occurred at much higher temperatures, low sulfur content solutions also exist. Righter et al. (2017) carried out phase equilibria experiments of Fe–Ni–S–C compositions and showed that low sulfur contents (~0.5 wt%) can crystallize at expected core–mantle boundary temperatures. A similar study has been carried out by Steenstra et al. (2017) who found that enough carbon can be partitioned into the core to lower the crystallization temperature of the inner core.

Several attempts have been made at modeling a lunar dynamo that consider core crystallization, but with different conclusions. These models have assumed a simplified core composition of iron alloyed with sulfur, which is the best studied alloying element at these pressures (e.g., Buono and Walker 2011). A description on how to parameterize inner core growth rates can be found in Nimmo (2015). Although the specific evolutions depend upon the evolution of the mantle, one main conclusion is that a long-lived, chemically driven dynamo is possible. Like the thermal core dynamos, the surface field strengths are predicted generally to be less than ~1 μT (e.g., Laneuville et al. 2014; Scheinberg et al. 2015; Evans et al. 2017).

Zhang et al. (2013) tested whether a dense ilmenite-rich layer at the base of the mantle could become thermally unstable and explain the observed timing and spatial distribution of mare volcanism. Such models imply strong cooling of the core when the layer becomes unstable, and they found an approximately 700-million-year time period with a high core–mantle boundary heat flow. In these models, the timing of inner core growth, which is a good proxy for the onset of a chemically driven dynamo, is controlled by the time it takes the ilmenite-rich layer surrounding the core to become unstable (cf. Zhang et al. 2017). Similar simulations by Scheinberg et al. (2015) showed that the effect of a thermal blanketing layer could delay dynamo generation by more than 500 million years and could also extend dynamo activity to about 1.5 Ga (Fig. 7). They further suggested that there may exist extended periods of time where the available power for dynamo generation remains close to zero, and therefore that small changes in the mantle convection pattern or lateral heterogeneities may stop and re-start the dynamo.

A different thermal model was developed by Laneuville et al. (2013, 2014), who considered that the majority of the heat-producing elements (i.e., KREEP) were located within the crust of the Procellarum KREEP terrane. For core sulfur contents from 2 to 8 wt%, core crystallization usually started before 4 Ga and the final solid inner core radius was about half that of the fluid core. Laneuville et al. (2018) made use of an improved inner core growth model and showed that dynamo activity would stop at about 3.5–3.7 Ga for a bulk core sulfur abundance of 4 wt%. This result is consistent with similar models by Scheinberg et al. (2015) who found that bulk core sulfur compositions between 2 and 8 wt% would be able to power a dynamo up until about 3.5 Ga for the most sulfur-rich compositions. As core crystallization proceeds, the sulfur content of the outer fluid core will necessarily increase. When the sulfur content in the fluid core exceeds about 7 wt%, the liquidus curve becomes less steep than the adiabatic temperature profile, and core crystallization would instead proceed from the top down (Laneuville et al. 2014). This transition from crystallizing at the inner-core boundary to the core–mantle boundary (the ‘iron snow’ regime) would likely stop dynamo activity after a few 100 Myr at best (Rückriemen et al. 2015).

4.3. Dynamos driven by mechanical forcing

In the previous two sections, we discussed dynamos driven by the cooling of either the core or a basal silicate magma ocean. In this section, we discuss dynamos that are instead powered by mechanical forcings such as precession, librations and changes in rotation rate following large impact events.

At present, the solid lunar mantle precesses around the normal to the ecliptic with a period of 18.6 years and an angle I_e of 1.54°. The liquid lunar core, however, does not track the precession of the mantle, because the mantle torques are currently too small (Meyer and Wisdom 2011); its mean rotation axis instead coincides approximately with the ecliptic normal. As a result, there is a differential motion between the mantle and the mean core, which can drive turbulent motions in the core fluid, and potentially a dynamo. Lunar laser ranging studies (Williams et al. 2001) have estimated a present-day differential velocity of 2–3 cm s^{-1} and a rate of dissipation of 60 MW (~0.04 mW m^{-2}). This dissipation rate is much less than the heat flow required to maintain an adiabatic core (between 2 and 10 mW m^{-2}), which may suggest that precession is not likely to drive a dynamo at present.

In the past, the Moon was closer to Earth, the rotation rate was greater, and I_e was larger (Ward 1975), leading to a larger dissipated power at the core–mantle boundary. At a distance a smaller than about 48 R_E, where R_E is the Earth mean radius, the power available would have exceeded the estimated adiabatic threshold (Dwyer et al. 2011). At even earlier times and distances ($a < 15$–$29\ R_E$), the mantle would have been sufficiently distorted that the core would have precessed with the mantle, and there would not have been enough differential motion to drive a dynamo (Meyer and Wisdom 2011, Ćuk et al. 2019). As the Moon evolved outwards, there was thus a period during which a precession-driven dynamo could have operated. One large uncertainty with this scenario concerns the timing of this period. Although the critical Earth–Moon distances are known, converting distance to time requires the evolution of the lunar orbit to be known. This depends mainly on the rate of dissipation in the Earth (Williams 2000), which at present is controlled by the detailed characteristics of the ocean basins (Egbert and Ray 2000). The transition distance of 48 R_E (beyond which dynamo activity probably ceased) has been estimated to have occurred 2–3 billion years ago (Fig.7; Dwyer et al. 2011).

A second uncertainty is whether the fluid flows driven by precession can drive a dynamo (e.g., Stevenson 1983). Dwyer et al. (2011) argued that the inferred differential motion was likely to result in turbulence, but their scaling arguments for the predicted surface dynamo field strength (few μT) were based on numerical models of convection driven dynamos (Christensen et al. 2009), as discussed in Section 4.1. More recent work has investigated both the likely flow patterns and the likely field strengths. While Noir and Cébron (2013) studied the influence of the core triaxial shape on laminar flows, Lin et al. (2015, 2016) used simulations in spheres to confirm that instabilities and turbulence are expected within the current lunar core. Such instabilities may generate large-scale vortices that are favorable to the generation of strong magnetic fields, especially in the past when the precession forcing was larger. Regardless, it remains hazardous to extrapolate these dynamo simulation results to the Moon, as they all neglect the ellipsoidal shape of the lunar core and the resulting core–mantle boundary topographic torque. A systematic numerical study by Cébron et al. (2019) shows that large-scale planetary magnetic fields are in fact unlikely to be produced by a precession-driven dynamo in a perfectly spherical core. In reality, the topographic torque resulting from the ellipsoidal core shape dominates the viscous torque in the lunar core. The relative magnitudes of the torques in these simulations are thus inconsistent. To mitigate these problems, we need dynamo simulations in ellipsoids at low viscosity, which is challenging.

Despite the uncertainties, a precession-driven dynamo has one large advantage over most of the other proposed mechanisms. Because it ultimately depends on the Moon's rotation, the power potentially available to drive a dynamo can be tens of GW (corresponding to more than 7 mW m^{-2} at the core–mantle boundary), far in excess of the power available to most other mechanisms. Moreover, the decrease of the precession-forcing with time could provide a natural mechanism to end the dynamo. This mechanism is thus a promising candidate to explain the early, high-field strength epoch of the Moon, and potentially the billion-year-old magnetic fields implied by paleomagnetism studies (Tikoo et al. 2017).

One can also drive differential rotation in the lunar core by tides or librations (Le Bars et al. 2015). Like precession, the current differential rotation at the core–mantle boundary due to librations is too small to generate dynamo action. However, impact-induced changes in the Moon's rotation rate in the past could have excited inertial instabilities in the fluid core, leading to short-lived dynamos (Le Bars et al. 2011). Basin-forming impact events are energetic enough to have unlocked the Moon from synchronous rotation (Wieczorek and Le Feuvre 2009). Since the lunar core would have initially kept rotating at the pre-impact synchronous rate, a strong differential rotation would have been generated at the core–mantle boundary that would have persisted for about 10,000 years, possibly powering a short-lived dynamo. One can thus imagine a series of short-lived dynamos early in lunar evolution when the large impact basins were forming. Impact-driven changes in rotation, however, are unlikely to have generated a dynamo after the final large impact that formed the Orientale basin at ~3.72 Ga (Suavet et al. 2013). Furthermore, because of the short durations of such dynamos, they are also unlikely to explain most of the lunar paleomagnetic data and crustal magnetization from before this time.

As with precession-driven dynamos, there are large uncertainties in the scenario of impact induced changes in rotation. One question is whether it is possible to excite three-dimensional inertial instabilities in a stably stratified lunar core. From a static point of view, one can see a density stratification as an energy barrier. However, from a dynamical point of view, density stratification can give rise to internal gravity waves, which can also be coupled, and result in parametric resonances of gravito-inertial waves. Density stratification is therefore not necessarily problematic for dynamo generation in the lunar core under this scenario (e.g., Cébron et al. 2010; Vidal et al. 2018).

Another key question is whether the fluid flows driven by inertial instabilities can drive a dynamo. Le Bars et al. (2011) argued that the inferred differential motion can generate turbulence, which is confirmed by simulations and experiments (Le Reun et al. 2017; Lemasquerier et al. 2017). Dynamos have been numerically obtained for mechanical forcings due to precession, librations and tides (Tilgner 2005; Wu and Roberts 2013; Cébron and Hollerbach 2014), and Le Bars et al. (2011) argued that the magnetic field could have reached several μT at the surface of the early Moon. However, just as for precession-driven dynamos, the extrapolation of the numerical results to the lunar parameter regime remains hazardous because it is based on poorly constrained scaling arguments.

Thermally driven dynamos can also be generated by the viscous heating associated with any mechanical forcing. Considering the Cassini state of a possible solid inner core, Stys and Dumberry (2020) showed that the power dissipated at the precessing inner core boundary could in fact exceed the power dissipated at the core–mantle boundary for Earth–Moon separations greater than 42 R_E. For inner core radii larger than 100 km, this heating is sufficient to generate a convection driven dynamo up until at least 50 R_E, and potentially to the present day. Even if their model neglects various feedbacks (such as among viscous heating, the mutual orientations of the spin vectors in the Cassini state, the orbital inclination, and electromagnetic coupling), it shows that the expected viscous heating is comparable to the heat released from inner core crystallization, which is the largest contribution to the core heat budget in the absence of precession. Growth of the solid inner core could thus have been significantly slowed, and such viscous heating at the inner core boundary should thus be included in thermal evolution models.

5. SYNTHESIS

Paleomagnetic studies of lunar samples and spacecraft analyses of the crustal magnetic field both indicate that the Moon once had a global magnetic field that was generated by an internal dynamo. The existence of pervasive deep magnetization in the ancient highlands crust implies that a global field was present as the crust cooled during the first 100 million years following its formation. Magnetic anomalies in the interiors of impact basins imply

that a global field must have been present during most of the Nectarian period (from ~4.1 to 3.89 Ga), and perhaps for parts of the older pre-Nectarian period as well. Sample analyses provide evidence for a dynamo as far back as 4.25 Ga to at least as young as 1.92 Ga, with the dynamo ceasing before 0.80 Ga (Fig. 3). If the dynamo operated continuously, as opposed to intermittently, dynamo activity could have existed during more than three-quarters of the Moon's evolution, which is extremely surprising given the relatively small size of the Moon in comparison to the other terrestrial planets. The now widespread acceptance of an extinct long-lived lunar dynamo is probably the key development since the time of writing of the first *New Views of the Moon* book over a decade ago.

If the existence of an ancient dynamo is all but assured, the temporal evolution of the field strength is less well constrained. Paleomagnetic field strengths derived using isothermal techniques are inherently uncertain by a multiplicative factor of about 2, and in many cases, only a strict upper limit on the paleointensity can be obtained. The time when the magnetization was acquired can sometimes also be uncertain, in some cases by more than hundreds of millions of years. Regardless, paleomagnetic analyses using modern methods allow for some firm conclusions to be drawn (Fig. 3). First, between 4.25 and 3.56 Ga, the surface field strength was comparable to that of Earth today, from about 40 to 110 μT (excluding uncertainties). Following this high-field epoch, the field strength decreased by more than an order of magnitude by 3.19 Ga to less than about 4 μT. An analysis of a rock using the double heating technique robustly demonstrates the existence of an ~5 μT field sometime between about 1 and 2 Ga. Lastly, double heating analyses of two young breccias indicate that the dynamo must have ceased before about 0.8 Ga.

Considerable progress has been made over the past decade towards understanding the energy sources that might be responsible for generating a long-lived dynamo. As shown in Figure 7, several mechanisms have been proposed and each of these may have contributed to powering the dynamo over different time periods. The mechanisms fall into three broad categories: convection driven by thermal sources, core crystallization, and mechanical dynamos related to precession and changes in lunar rotation.

Secular cooling of the Moon (the first scenario) could have driven convection in the core and powered a dynamo. Such a dynamo could occur just after Moon formation and last up to about 4 Ga. The duration of this dynamo could be extended if the mantle viscosity was reduced by the presence of water or if a dense KREEP-rich layer surrounded the core. These models all predict that the core should at some point begin to crystallize (the second scenario), and the buoyancy related to the liberation of light alloying elements along with the release of latent heat could prolong dynamo activity. Core crystallization could sustain continuously a dynamo up to about 3.5 Ga for standard convection models, or up to about 1.5 Ga for models that include an early thermal blanketing layer that surrounds the core. Furthermore, some of these models predict that the dynamo could have been reactivated at later times for short time periods (~100 My). A related model is that dynamo generation could have perhaps occurred instead in a long-lived basal silicate magma ocean. A dynamo powered by thermal convection in the fluid core (or a basal magma ocean) combined with later core crystallization could magnetize the ancient highlands crust and the interiors of the large basins.

An alternative third scenario is that a dynamo could be powered by mechanical forcing of the core by topographic torques associated with the core–mantle boundary. In these models, differential rotation between the solid mantle and fluid core (or solid inner core and fluid core) generates instabilities that lead to turbulent three-dimensional flows. In one model, the instabilities are excited by precession of the mantle spin axis. Precession of the fluid core could potentially generate a dynamo early in the Moon's orbital evolution, continuing until about 2 Ga. The heat dissipated by a precessing solid inner core (if present) core could continue to drive convective motions, perhaps up until the present day. For precession dynamos, the time-evolution of the Moon's magnetic field could be used to constrain the orbital evolution

of the Moon. This model is attractive in that the power that is available to drive the dynamo is large, being derived from the Moon's rotation. In another model, instabilities are excited by a change in the mantle rotation rate following large basin-forming impacts. These flows could conceivably generate a short-lived dynamo that lasts about 10,000 years, and the last such dynamo would have occurred at about 3.7 Ga when the last large impact basin formed. Although short-lived, such dynamos could magnetize the impact melt sheets of the basins that were responsible for altering the Moon's rotation rate.

The origins of the magnetization responsible for the crustal magnetic fields are now better understood as a result of global magnetic field mapping from orbit. Analyses of the weak fields that are omnipresent over the highlands imply that magnetization there is located more than 10 km below the surface. This deep magnetization is most plausibly related to small quantities of metallic iron derived from the magma ocean at the time of crust formation. The largest concentration of strong magnetic anomalies is located on the northern rim of the farside South Pole–Aitken basin. Based on geologic evidence for this basin having formed under oblique impact conditions, these anomalies may instead be related to iron-rich remnants of the projectile that formed this basin. Alternatively, these anomalies could be the result of iron-rich ejecta that were concentrated at the antipodes of a few nearside impact basins, where the enhanced iron abundances are also a result of remnants of the projectiles that formed these basins. Some Nectarian-aged impact basins have magnetic anomalies in their interiors, and these anomalies are confined largely to within the basin's inner depression where a several-km thick impact melt sheet is predicted to reside. The magnitudes of these anomalies are consistent with less than a wt% of metallic iron derived from the impactor that formed the basin.

6. OUTSTANDING QUESTIONS

Despite the advances that have been made over the past decade in lunar magnetism, there remain unresolved problems of fundamental importance. The first is that current dynamo models are incapable of accounting for most surface field strengths obtained by paleomagnetic analyses. Nearly all dynamo models predict field strengths that are on the order of a μT, but the measured field strengths between 4.25 and 3.56 Ga are 1–2 orders of magnitude larger. At best, the core thermal and crystallization dynamo models can account only for the weakest field strengths after about 3.5 Ga (Fig. 3). Convection in a silicate basal magma ocean could perhaps generate larger surface field strengths (as a result of its proximity to the surface), but it is difficult for molten silicate materials to obtain the required electrical conductivities for dynamo generation. All dynamo models make use of similar scaling relationships between power and magnetic field strength, where this scaling relation is based on numerical simulations of Earth-like dynamos that involve thermal and compositional buoyancy sources. Although one might expect that this scaling would hold for similarly driven dynamos on the Moon, it is unknown if these relations are appropriate for mechanically driven dynamos.

A second question is that it is difficult to understand how the dynamo field strength could have dropped by at least an order of magnitude after 3.56 Ga, and then persisted in this weakened state until at least 1.92 Ga. It is possible that this transition corresponds to a change in the dominant source of energy powering the dynamo. Some combination of thermal convection, core crystallization, precession, and impact-induced changes in rotation could have operated concurrently for extended periods of lunar evolution. However, dynamo simulations have yet to model how the flows induced by each mechanism would interact. The power scaling may not be simply a linear addition of the individual sources, and it is not clear if the dynamo field would be primarily dipolar and aligned with the Moon's rotation axis.

A third outstanding problem is the origin of the strongest lunar magnetic anomalies. Some of the strongest and largest concentrations of anomalies are plausibly related to metallic iron

delivered to the Moon during impact processes. Nevertheless, there are many isolated magnetic anomalies that have no clear correlation with known geologic processes. One prominent example is the nearside Reiner-γ anomaly which has no topographic, gravitational, or compositional signature (apart from the surficial swirl deposits). The only possible correlation with geology is its proximity to the Marius Hills volcanic complex. An additional example is the Descartes anomaly, which is close to the Apollo 16 landing site. Although the surface of this region is covered by ejecta from the Imbrium basin, the vast majority of Imbrium impact deposits have considerably weaker field strengths. It is possible that these isolated anomalies could be the result of distal iron-rich impact ejecta from large impact events, but if so, it would probably not be possible to determine from which basin these deposits originated, nor their age. It is possible that these anomalies could be the result of local enhancements in the iron abundance of the crust at the time of crust formation, but the process by which this could occur is unknown. It is also possible that these anomalies could be the result of magnetized crustal intrusions, but this is difficult to test, as most anomalies are not associated with volcanic features.

Lastly, there is a potential contradiction between the duration of the epoch of high field strengths as obtained from paleomagnetic analyses (from ~4.25 to 3.56 Ga) and the magnetic signature of the crust. If the high field strengths extended into the early and late Imbrian epochs, then one might expect that impact basins formed in this period would be magnetized, as are many of the Nectarian aged basins. However, of the three basins that formed in the Imbrian period (Imbrium, Orientale, and Schrödinger), none of these are strongly magnetized. The Imbrium basin is associated with some of the weakest magnetic fields on the Moon, the Orientale impact basin is relatively demagnetized with respect to the surrounding crust, and the Schrödinger basin possesses only very weak field strengths. One possibility is that these basins formed under moderately oblique conditions and that the iron-rich projectile materials were deposited outside of the basin rim. Alternatively, it is possible that the projectiles themselves were iron poor. Investigations of the magnetic signatures of smaller impact craters as a function of age might help constrain how the dynamo field strength varied in time.

Progress on understanding lunar magnetism will be made by a combination of numerical dynamo simulations, continued paleomagnetic analyses of lunar rocks, and improved high-resolution magnetic field mapping from orbital data. First, numerical simulations of precession driven dynamos are relatively unexplored, and do not yet properly take into account the topographic torques associated with the triaxial core–mantle boundary. Further simulations should be able to determine if precession dynamos generate stronger fields than buoyancy driven dynamos, and how long such a dynamo could operate. Second, only about a dozen paleomagnetic analyses have been performed to date on lunar samples using modern analysis techniques, and of these, only a few have successfully used the Thellier–Thellier double heating technique. As a result, the time evolution of the surface field strength is poorly constrained for several key time periods. Continued analysis of the existing lunar sample collection should help constrain when the dynamo started, when the transition from high to low field strengths occurred, whether dynamo activity was continuous or intermittent, and when the dynamo turned off. Third, the spatial correlation length of crustal magnetism is poorly constrained. The correlation length is closely related to the origin, geometry and depth of the magnetic sources, and is not easily determined from existing orbital data tens of km above the surface. Surface measurements made during the Apollo missions as well as analyses of swirl morphology have in fact shown that the field direction can change substantially over km length scales.

Fundamental advances in lunar magnetism will also be made by the collection of new samples. All of the paleomagnetic measurements that have been made so far are from rocks derived from a small geographic extent on the lunar surface. Future sampling for paleomagnetic analyses should focus on obtaining samples far from the nearside equatorial zone of Apollo and on obtaining both old and young samples. One ideal target would be the South Pole–Aitken

basin, which is not only the oldest impact basin on the Moon, but which also hosts a large range of smaller impact basins with ages extending into the late Imbrian. Another ideal target would be of young (<2 Ga) basaltic lava flows on the nearside. The collection of oriented samples derived from bedrock would be a major advance that would provide direct information about the geometry of the dynamo field and the location of the magnetic pole. Storage of these samples in a long-term low magnetic-field environment would be a technically easy and cost-effective solution to avoid the VRM contamination that is present in all of the curated Apollo samples.

7. CONCLUSIONS

Paleomagnetic analyses of lunar rocks and magnetic field mapping from orbit reveal a surprising magnetic history for Earth's moon. An internal dynamo appears to have operated (at least intermittently) for about three-quarters of lunar evolution, with the field strengths being surprisingly strong (Earth-like) for the first billion years. The dynamo may have been powered in the core by traditional mechanisms such as thermo-compositional convection or more novel drivers such as mantle precession that are unlike those responsible for the dynamo of Earth. Though the dynamo is likely to have originated in the fluid metallic core, dynamo activity in a silicate basal magma ocean cannot be excluded. Many strong magnetic anomalies exist, of which some may be related to asteroidal materials that were accreted to the Moon during basin-forming impacts, while others have no obvious correlation with geologic processes. All of these observations are surprising given the small relative size of the core of the Moon, and the low abundance of magnetic minerals that are found in most lunar rocks.

As a well-studied body, the Moon is a touchstone for processes that may have, or continue to, operate on the other terrestrial planets and moons. All planets and moons suffered billions of years of impact cratering, and many also have active or extinct intrinsic magnetic fields. The accretion of iron-rich projectile materials to the surfaces of these bodies (perhaps later oxidized) could be partially responsible for some of the magnetic anomalies discovered on Mercury and Mars. The shock waves associated with large impacts could also act to both magnetize or demagnetize planetary crusts across the solar system. In addition, determination of the lunar magnetic field's behavior with time may help elucidate the history of the geodynamo. The Moon is, and will continue to be, a natural laboratory for studying the magnetic processes that operate on the other terrestrial planets and moons of our solar system as well as the vast diversity of exoplanets.

ACKNOWLEDGMENTS

We thank two anonymous reviewers for their thoughtful comments that helped improve the clarity of this manuscript. MAW, JG and DC were supported by the French Agence Nationale de la Recherche (grant ANR-14-CE33-0012). BPW thanks the NASA Solar System Workings and Planetary Major Equipment Programs (grant NNX15AL62G) and the NASA Solar System Exploration Research Virtual Institute node at Brown-MIT (grant NNA14AB01A).

REFERENCES

Almeida, TP, Muxworthy AR, Kovács, A, Williams, W, Brown PD, Dunin-Borkowski RE (2016) Direct visualization of the thermomagnetic behavior of pseudo–single-domain magnetite particles. Sci Adv 2:E1501801

Anderson KA, Lin RP, McGuire RE, McCoy JE (1975) Measurement of lunar and planetary magnetic fields by reflection of low energy electrons. Space Sci Inst 1:439–470

Andrews-Hanna JC, Asmar SW, Head JW, Kiefer WS, Konopliv AS, Lemoine FG, Matsuyama I, Mazarico E, McGovern PJ, Melosh HJ, Neumann GA, Nimmo F, Phillips RJ, Smith DE, Solomon SC, Taylor GJ, Wieczorek MA, Williams JG, Zuber MT (2013) Ancient igneous intrusions and early expansion of the Moon revealed by GRAIL gravity gradiometry. Science 339:675–678

Andrews-Hanna JC, Weber RC, Garrick-Bethell I, Evans AJ, Kiefer WS, Grimm RE, Keane JT, Laneuville M, Ishihara Y, Kamata S, Matsuyama I (2023) The structure and evolution of the lunar interior. Rev Mineral Geochem 89:243–292

Antonangeli D, Morard G, Schmerr NC, Komabayashi T, Krisch M, Fiquet G, Fei Y (2015) Toward a mineral physics reference model for the Moon's core. PNAS 112:3916–3919

Arkani-Hamed J, Boutin D (2014) Analysis of isolated magnetic anomalies and magnetic signatures of impact craters: Evidence for a core dynamo in the early history of the Moon. Icarus 237:262–277

Arkani-Hamed J, Boutin D (2017) South Pole–Aitken basin magnetic anomalies: Evidence for the true polar wander of Moon and a lunar dynamo reversal. J Geophys Res 122:1195–1216

Baek S-M, Kim KK, I Garrick-Bethell, Jin H, Lee J-K, Lee H-J (2017) Detailed study of the Mare Crisium northern magnetic anomaly. J Geophys Res 122:411–430

Bamford RA, Alves EP, Cruz F, Kellett BJ, Fonseca RA, Silva LO, Trines RM, Halekas JS, Kramer G, Harnett E, Cairns RA (2016) 3D pic simulations of collisionless shocks at lunar magnetic anomalies and their role in forming lunar swirls. Astrophys J 830:146

Berndt TA, Chang L (2018) Theory of stable multidomain thermoviscous remanence based on repeated domain wall jumps. J Geophys Res 123:10,3990–10,417

Blewett DT, Coman EI, Hawke BR, Gillis-Davis JJ, Purucker ME, Hughes CG (2011) Lunar swirls: Examining crustal magnetic anomalies and space weathering trends. J Geophys Res 116:E02002

Buono AS, Walker D (2011) The Fe-rich liquidus in the Fe–FeS system from 1 bar to 10 GPa. Geochim Cosmochim Acta 75:2072–2087

Buz J, Weiss BP, Tikoo SM, Shuster DL, Gattacceca J, Grove TL (2015) Magnetism of a very young lunar glass. J Geophys Res 120:1720–1735

Cébron D, Hollerbach R (2014) Tidally driven dynamos in a rotating sphere. Astrophys J 789:L25

Cébron D, Maubert P, Le Bars M (2010) Tidal instability in a rotating and differentially heated ellipsoidal shell. Geophys J Int 182:1311–1318

Cébron D, Laguerre R, Noir J, Schaeffer N (2019) Precessing spherical shells: flows, dissipation, dynamo and the lunar core. Geophy J Int, 219:S34-S57

Christensen UR (2010) Dynamo scaling laws and applications to the planets. Space Sci Rev 152:565–90

Christensen U (2019) Planetary magnetic fields and dynamos. Oxford Research Encyclopedia of Planetary Science, https://oxfordre.com/planetaryscience/

Christensen UR, Aubert J (2006) Scaling properties of convection-driven dynamos in rotating spherical shells and application to planetary magnetic fields. Geophys J Int 166:97–114

Christensen UR, Holzwarth V, Reiners A (2009) Energy flux determines magnetic field strength of planets and stars. Nature 457:167–169

Constable C, Korte M, Panovska S (2016) Persistent high paleosecular variation activity in southern hemisphere for at least 10000 years. Earth Planet Sci Lett 453:78–86

Cournède C, Gattacceca J, Rochette P (2012) Magnetic study of large Apollo samples: Possible evidence for an ancient centered dipolar field on the Moon. Earth Planet Sci Lett 331–332:31–42

Cromwell G, Tauxe L, Halldorsson SA (2015) New paleointensity results from rapidly cooled Icelandic lavas: Implications for Arctic geomagnetic field strength. J Geophys Res 120:2913–2934

Ćuk M, Hamilton DP, Stewart ST (2019) Early dynamics of the lunar core. J Geophys Res 124:2917–2928

Deca J, Divin A, Lue C, Ahmadi T, Horányi M (2018) Reiner Gamma albedo features reproduced by modeling solar wind standoff. Commun Physics 1:12

Deca J, Hemingway DJ, Divin A, Lue C, Poppe AR, Garrick-Bethell I, Lembège B, Horányi M (2020) Simulating the Reiner Gamma swirl: the long-term effect of solar wind standoff. J Geophys Res 125:e2019JE006219

Denevi BW, Robinson MS, Boyd AK, Blewett DT, Klima RL (2016) The distribution and extent of lunar swirls. Icarus 273:53–67

Dolginov SS, Eroshenko EG, Zhuzgov L, Pushkov N (1966) Measurements of the magnetic field near the Moon by the Luna 10 orbiter. Dokl Acad Sci USSR, Earth Sci Sect 170:18–20

Dolginov SS, Eroshenko EG, Sharova VA, Vnuchkova TA, Vanian LL, Okuleskii BA, Bazilevskii AT (1976) Study of magnetic field, rock magnetization and lunar electrical conductivity in the Bay Le Monnier. Moon 15:3–14

Dunn JR, Fuller M (1972) Thermoremanent magnetization (TRM) of lunar samples. Moon 4:49–62

Dwyer CA, Stevenson DJ, Nimmo F (2011) A long-lived lunar dynamo driven by continuous mechanical stirring. Nature 479:212–214

Dyal P, Parkin CW, Daily WD (1974) Magnetism and the interior of the Moon. Rev Geophys Space Phys 12:568–591

Egbert GD, Ray RD (2000) Significant dissipation of tidal energy in the deep ocean inferred from satellite altimeter data. Nature 405:775–778

Einsle JF, Harrison RJ, Kasama T, Conbhuí PO, Fabian K, Williams W, Woodland L, Fu RR, Weiss BP, Midgley PA (2016) Multi-scale three-dimensional characterization of iron particles in dusty olivine: Implications for paleomagnetism of chondritic meteorites. Am Mineral 101:2070–2084

Elkins-Tanton LT, Grove TL (2011) Water (hydrogen) in the lunar mantle: Results from petrology and magma ocean modeling. Earth Planet Sci Lett 307:173–179

Evans AJ, Zuber MT, Weiss BP, Tikoo SM (2014) A wet, heterogeneous lunar interior: Lower mantle and core dynamo evolution. J Geophys Res 119:1061–1077
Evans AJ, Tikoo SM, Andrews-Hanna JC (2017) The case against an early lunar dynamo powered by core convection. Geophys Res Lett 45
Fuller M (1974) Lunar magnetism. Rev Geophys Space Phys 12:23–70
Fuller M (1998) Lunar magnetism: A retrospective view of the Apollo sample magnetic studies. Phys Chem Earth 23:725–735
Fuller M, Cisowski SM (1987) Lunar paleomagnetism. Geomagnetism 2:307–455
Garcia RF, Gagnepain-Beyneix J, Chevrot S, Lognonné P (2011) Very preliminary reference Moon model. Phys Earth Planet Inter 188:96–113
Garrick-Bethell I, Zuber MT (2009) Elliptical structure of the lunar South Pole–Aitken basin. Icarus 204:399–408
Garrick-Bethell I, Weiss BP (2010) Kamacite blocking temperatures and applications to lunar magnetism. Earth Planet Sci Lett 294:1–7
Garrick-Bethell I, Kelley MR (2019) Reiner Gamma: A magnetized elliptical disk on the Moon. Geophys Res Lett 46:5065–5074
Garrick-Bethell I, Weiss BP, Shuster DL, Buz J (2009) Early lunar magnetism. Science 323:356–359
Garrick-Bethell I, Head JW, Pieters CM (2011) Spectral properties, magnetic fields, and dust transport at lunar swirls. Icarus 212:480–492
Garrick-Bethell I, Perera V, Nimmo F, Zuber MT (2014) The tidal–rotational shape of the Moon and evidence for polar wander. Nature 512:181–184
Garrick-Bethell I, Weiss BP, Shuster DL, Tikoo SM, Tremblay MM (2017) Further evidence for early lunar magnetism from troctolite 76535. J Geophys Res 122:76–93
Garrick-Bethell I, Poppe AR, Fatemi S (2019) The lunar paleo-magnetosphere: implications for the accumulation of polar volatile deposits. Geophys Res Lett 46:5778–5787
Gattacceca J, Rochette P (2004) Toward a robust normalized magnetic paleointensity method applied to meteorites. Earth Planet Sci Lett 227:377–393
Gattacceca J, Boustie M, Hood L, Cuq-Lelandais J-P, Fuller M, Bezaeva NS, de Resseguier T, Berthe L (2010) Can the lunar crust be magnetized by shock: Experimental groundtruth. Earth Planet Sci Lett 299:42–53
Gong S, Wieczorek MA (2020) Is the lunar magnetic field correlated with gravity or topography? J Geophys Res 125:e2019JE006274
Gose WA, Strangway DW, Pearce GW (1973) A determination of the intensity of the ancient lunar magnetic field. Moon 7:198–201
Grimm RE (2013) Geophysical constraints on the lunar Procellarum KREEP Terrane. J Geophys Res 118:768–777
Halekas JS, Mitchell DL, Lin RP, Frey S, Hood LL, Acuña MH, Binder AB (2001) Mapping of crustal magnetic anomalies on the lunar near side by the Lunar Prospector electron reflectometer. J Geophys Res 106:27841–27852
Halekas JS, Mitchell DL, Lin RP, Hood LL, Acuña MH, Binder AB (2002) Demagnetization signatures of lunar impact craters. Geophys Res Lett 29:1645
Halekas JS, Lin RP, Mitchell DL (2003) Magnetic fields of lunar multi-ring impact basins. Meteorit Planet Sci 38:565–578
Halekas JS, Lillis RJ, Lin RP, Manga M, Purucker ME, Carley RA (2010) How strong are lunar crustal magnetic fields at the surface? Considerations from a reexamination of the electron reflectometry technique. J Geophys Res 115:E03006
Halekas JS, Delory GT, Farrell WM, Angelopoulos V, McFadden JP, Bonnell JW, Fillingim MO, Plaschke F (2011) First remote measurements of lunar surface charging from ARTEMIS: Evidence for nonmonotonic sheath potentials above the dayside surface. J Geophys Res 116:A07103
Harada Y, Machida S, Saito Y, Yokota S, Asamura K, Nishino MN, Tsunakawa H, Shibuya H, Takahashi F, Matsushima M, Shimizu H (2013) Small-scale magnetic fields on the lunar surface inferred from plasma sheet electrons. Geophys Res Lett 40:3362–3366
Heiken, G, Vaniman DT, French BM (ed.) (1991) Lunar Sourcebook: A User's Guide to the Moon. Cambridge University Press, Cambridge
Hemingway D, Garrick-Bethell I (2012) Magnetic field direction and lunar swirl morphology: Insights from Airy and Reiner Gamma. J Geophys Res 117:E10012
Hemingway DJ, Tikoo SM (2018) Lunar swirl morphology constrains the geometry, magnetization, and origins of lunar crustal magnetic anomalies, J Geophys Res 123
Hood LL (1981) Sources of lunar magnetic anomalies and their bulk directions of magnetization—Additional evidence from Apollo orbital data. Proc Lunar Planet Sci Conf 12:817–830
Hood LL (1986) Geophysical constraints on the lunar interior. In: Origin of the Moon. Hartmann WK, Phillips RJ, Taylor GJ (eds) Lunar and Planet Inst, p 361–410
Hood L L (1987) Magnetic field and remanent magnetization effects of basin-forming impacts on the Moon. Geophys Res Lett 14:844–847
Hood LL (1995) Frozen fields. Earth Moon Planets 67:131–142
Hood LL (2011) Central magnetic anomalies of Nectarian-aged lunar impact basins: Probable evidence for an early core dynamo. Icarus 211:1109–1128

Hood LL, Huang Z (1991) Formation of magnetic anomalies antipodal to lunar impact basins: Two-dimensional model calculations. J Geophys Res 96:9837–9846
Hood LL, Schubert G (1980) Lunar magnetic anomalies and surface optical properties. Science 208:49–51
Hood LL, Spudis PD (2016) Magnetic anomalies in the Imbrium and Schrödinger impact basins: Orbital evidence for persistence of the lunar core dynamo into the Imbrian epoch. J Geophys Res 121:2268–2281
Hood LL, Vickery A (1984) Generation of transient magnetic fields in hypervelocity meteoroid impacts with application to lunar paleomagnetism. J Geophys Res 89:C211-C223
Hood LL, Williams CR (1989) The lunar swirls: Distribution and possible origins. Proc Lunar Planet Sci Conf 19:2737–2749
Hood LL, Artemieva NA (2008) Antipodal effects of lunar basin-forming impacts: Initial 3D simulations and comparisons with observations. Icarus 193:485–502
Hood LL, Richmond NC, Spudis PD (2013) Origin of strong lunar magnetic anomalies: Further mapping and examinations of LROC imagery in regions antipodal to young large impact basins. J Geophys Res 118:1265–1284
Hughes HG, App FN, McGetchin TR (1977) Global seismic effects of basin-forming impacts. Phys Earth Planet Inter 15:251–263
Jolliff BJ, Gillis JJ, Haskin LA, Korotev RL, Wieczorek MA (2000) Major lunar crustal terranes: Surface expressions and crust-mantle origins. J Geophys Res 105:4197–4216
Karato S-I (2013) Geophysical constraints on the water content of the lunar mantle and its implications for the origin of the Moon. Earth Planet Sci Lett 384:144–153
Keane JT, Matsuyama I (2014) Evidence for lunar true polar wander and a past low-eccentricity, synchronous lunar orbit. Geophys Res Lett 41:6610–6619
Khan A, Connolly JAD, Pommier A, Noir J (2014) Geophysical evidence for melt in the deep lunar interior and implications for lunar evolution. J Geophys Res 119:2197–2221
Kletetschka G, Wieczorek MA (2017) Fundamental relations of mineral specific magnetic carriers for paleointensity determination. Phys Earth Planet Inter 272:44–49
Kletetschka G, Kohout T, Wasilewski P (2003) Magnetic remanence in the Murchison meteorite. Meteorit Planet Sci 38:399–405
Kletetschka G, Acuña MH, Kohout T, Wasilewski PJ, Connerney JEP (2004) An empirical scaling law for acquisition of thermoremanent magnetization. Earth Planet Sci Lett 226:521–528
Klima R, Cahill J, Hagerty J, Lawrence D (2013) Remote detection of magmatic water in Bullialdus Crater on the Moon. Nature Geosci 6:73
Konrad W, Spohn T (1997) Thermal history of the Moon–implications for an early core dynamo and post-accretional magmatism. Adv Space Res 10:1511–1521
Korotev RL (2000) The great lunar hot spot and the composition and origin of the Apollo mafic ("LKFM") impact-melt breccias. J Geophys Res 105:4317–4346
Laneuville M, Wieczorek MA, Breuer D, Tosi N (2013) Asymmetric thermal evolution of the Moon. J Geophys Res 118:1435–1452
Laneuville M, Wieczorek MA, Breuer D, Albert J, Morard G, Rückriemen T (2014) A long-lived lunar dynamo powered by core crystallization. Earth Planet Sci Lett 40:251–260
Laneuville M, Taylor J, Wieczorek MA (2018) Distribution of radioactive heat sources and thermal history of the Moon. J Geophys Res: Planets 123:3144–3166
Lawrence K, Johnson C, Tauxe L, Gee JS (2008) Lunar paleointensity measurements: Implications for lunar magnetic evolution. Phys Earth Planet Inter 168:71–87
Le Bars M, Wieczorek M A, Karatekin Ö, Cébron D, Laneuville M (2011) An impact-driven dynamo for the early Moon. Nature 479:215–218
Le Bars M, Cébron D, Le Gal P (2015) Flows driven by libration, precession, and tides. Ann Rev Fluid Mech 47:163–193
Le Reun T, Favier B, Barker AJ, Le Bars M (2017) Inertial wave turbulence driven by elliptical instability. Phys Rev Lett 119:034502
Lemasquerier D, Grannan AM, Vidal J, Cébron D, Favier B, Le Bars M, Aurnou JM (2017) Libration-driven flows in ellipsoidal shells. J Geophys Res 122:1926–1950
Lepaulard C, Gattacceca J, Uehara M, Rochette P, Quesnel Y, Macke RJ SJ, Kiefer W (2019) A survey of the natural remanent magnetization and magnetic susceptibility of Apollo whole rocks. Phys Earth Planet Inter 290:36–43
Lin RP (1979) Constraints on the origins of lunar magnetism from electron reflection measurements of surface magnetic fields. Phys Earth Planet Int 20:271–280
Lin RP, Anderson KA, Hood L (1988) Lunar surface magnetic field concentrations antipodal to young large impact basins. Icarus 74:529–541
Lin Y, Marti P, Noir J (2015) Shear-driven parametric instability in a precessing sphere. Phys Fluids 27:046601
Lin Y, Marti P, Noir J, Jackson A (2016) Precession-driven dynamos in a full sphere and the role of large scale cyclonic vortices. Phys Fluids 28:066601
Matsuyama I, Nimmo F, Keane JT, Chan NH, Taylor GJ, Wieczorek MA, Kiefer WS, Williams JG (2016) GRAIL, LLR, and LOLA constraints on the interior structure of the Moon. Geophys Res Lett 43:8365–8375
Maxwell RE, Garrick-Bethell I (2020) Evidence for an ancient near-equatorial lunar dipole from higher precision inversions of crustal magnetization. J Geophys Res 125:e2020JE006567

McCubbin FM, Jolliff BL, Nekvasil H, Carpenter, PK, Zeigler RA, Steele A, Elardo SM, Lindsley DH (2011) Fluorine and chlorine abundances in lunar apatite: Implications for heterogeneous distributions of magmatic volatiles in the lunar interior. Geochim Cosmochim Acta 75:5073-5093
McCubbin FM, Vander Kaaden KE, Tartèse R, Klima RL, Liu Y, Mortimer J, Barnes JJ, Shearer CK, Treiman AH, Lawrence DJ, Elardo SM, Hurley DM, Boyce JW, Anand M (2015) Magmatic volatiles (H, C, N, F, S, Cl) in the lunar mantle, crust, and regolith: Abundances, distributions, processes, and reservoirs. Am Mineral 100:1668–1707
Meyer J, Wisdom J (2011) Precession of the lunar core. Icarus 211:921–924
Mighani S, Wang H, Shuster DL, Borlina CS, Nichols CIO, Weiss BP (2020) The end of the lunar dynamo. Sci Adv 6:eaax0883
Mitchell DL, Halekas JS, Lin RP, Frey S, Hood LL, Acuña MH, Binder A (2008) Global mapping of lunar crustal magnetic fields by Lunar Prospector. Icarus 194:401–409
Muxworthy AR, Williams W (2015) Critical single-domain grain sizes in elongated iron particles: implications for meteoritic and lunar magnetism. Geophys J Int 202:578–583
Nagy L, Williams W, Tauxe L, Muxworthy AR, Ferreira I (2019) Thermomagnetic recording fidelity of nanometer-sized iron and implications for planetary magnetism. PNAS 116:1984–1991
Nayak M, Hemingway D, Garrick-Bethell I (2017) Magnetic anomalies of the South Pole–Aitken Basin: Implications for true polar wander and the history of the lunar dynamo. Icarus 286:153–192
Neumann GA, Zuber, MT, Wieczorek MA, Head JW, Baker DMH, Solomon SC, Smith DE, Lemoine FG, Mazarico E, Sabaka TJ, Goossens SJ, Melosh HJ, Phillips RJ, Asmar SW, Konopliv AS, Williams JG, Sori MM, Soderblom JM, Miljković K, Andrews-Hanna JC, Nimmo F, Kiefer WS (2015) Lunar impact basins revealed by Gravity Recovery and Interior Laboratory measurements. Sci Adv 1:e1500852
Nicholas JB, Purucker ME, Sabaka TJ (2007) Age spot or youthful marking: Origin of Reiner Gamma. Geophys Res Lett 34:L02205
Nimmo F (2015) Energetics of the core. Treatise Geophys (second edition) 8:27–55
Noir J, Cébron D (2013) Precession-driven flows in non-axisymmetric ellipsoids. J Fluid Mech 737:412–439
Oliveira JS, Wieczorek MA (2017) Testing the axial dipole hypothesis for the moon by modeling the direction of crustal magnetization. J Geophys Res 122:383–399
Oliveira JS, Wieczorek MA, Kletetschka G (2017) Iron abundances in lunar impact basin melt sheets from orbital magnetic field data. J Geophys Res 122:2429–2444
Oran R, Weiss BP, Shprits Y, Miljković K, Tóth G (2020) Was the Moon magnetized by impact plasmas? Sci Adv 6:eabb1475
Oruba, L, Dormy, E (2014) Transition between viscous dipolar and inertial multipolar dynamos. Geophys Res Lett 41:7115–7120
Parker RL (1991) A theory of ideal bodies for seamount magnetism. J Geophys Res 96:16,101–16,112
Parmentier EM, Zhong S, Zuber MT (2002) Gravitational differentiation due to initial chemical stratification: origin of lunar asymmetry by the creep of dense KREEP? Earth Planet Sci Lett 201:473–480
Pearce GW, Gose WA, Strangway DW (1973) Magnetic studies on Apollo 15 and 16 lunar samples. Proc Lunar Sci Conf 4:3045–3076
Pearce GW, Hoye GS, Strangway DW (1976) Some complexities in the determination of lunar paleointensities. Proc Lunar Sci Conf 7:3271–3297
Pommier A, Leinenweber K, Tasaka M (2015) Experimental Investigation of the electrical behavior of olivine during partial melting under pressure and application to the lunar mantle. Earth Planet Sci Lett 425:242–255
Purucker ME (2008) A global model of the internal magnetic field of the Moon based on Lunar Prospector magnetometer observations. Icarus 197:19–23
Purucker ME, Nicholas JB (2010) Global spherical harmonic models of the internal magnetic field of the Moon based on sequential and coestimation approaches. J Geophys Res 115: E12007
Purucker ME, Head JW III, Wilson L (2012) Magnetic signature of the lunar South Pole–Aitken basin: Character, origin, and age. J Geophys Res 117:E05001
Rai N, van Westrenen W (2014) Lunar core formation: New constraints from metal–silicate partitioning of siderophile elements. Earth Planet Sci Lett 388:343–352
Ravat D, Purucker ME, Olsen N (2020) Lunar magnetic field models from Lunar Prospector and SELENE/Kaguya along-track magnetic field gradients. J Geophys Res 125, e2019JE006187
Richmond NC, Hood LL (2008) A preliminary global map of the vector lunar crustal magnetic field based on Lunar Prospector magnetometer data. J Geophys Res 113:E02010
Righter K, Go BM, Pando KA, Danielson L, Ross DK, Rahman Z, Keller LP (2017) Phase equilibria of a low S and C lunar core: Implications for an early lunar dynamo and physical state of the current core. Earth Planet Sci Lett 463:323–332
Rochette P, Gattacceca J., Ivanov AV, Nazarov MA, Bezaeva NS (2010) Magnetic properties of lunar materials: meteorites, Luna and Apollo returned samples. Earth Planet Sci Lett 292:383–391
Rückriemen T, Breuer D, Spohn T (2015), The Fe snow regime in Ganymede's core: a deep-seated dynamo below a stable snow zone. J Geophys Res 120:1095–1118
Runcorn SK (1982) Primeval displacements of the lunar pole. Phys Earth Planet Inter 29:135–147
Runcorn SK (1983) Lunar magnetism, polar displacements and primeval satellites in the Earth–Moon system. Nature 304:589–596

Runcorn SK (1996) The formation of the lunar core. Geochim Cosmochim Acta 69:1205–1208
Saal AE, Hauri EH, Cascio ML, Van Orman JA, Rutherford MC, Cooper RF (2008) Volatile content of lunar volcanic glasses and the presence of water in the Moon's interior. Nature 454:192–195
Schmidt PW, McEnroe SE, Clark DA, Robinson P (2007) Magnetic properties and potential field modeling of the Peculiar Knob metamorphosed iron formation, South Australia: An analog for the source of the intense Martian magnetic anomalies? J Geophys Res 112:B03102
Schmitt H. H. N. E. Petro R. A. Wells M. S. Robinson B. P. Weiss C. M. Mercer (2017) Revisiting the field geology of Taurus-Littrow. Icarus 298:2–33
Scheinberg AL, Soderlund KM, Schubert G (2015) Magnetic field generation in the lunar core: The role of inner core growth. Icarus 254:62–71
Scheinberg AL, Soderlund KM, Elkins-Tanton LT (2018) A basal magma ocean dynamo to explain the early lunar magnetic field. Earth Planet Sci Lett 492:144–151
Schubert G, Lichtenstein BR (1974) Observations of Moon-plasma interactions by orbital and surface experiments. Rev Geophys Space Phys 12:592–626
Schultz PH, Gault DE (1975) Seismic effects from major basin formations on the Moon and Mercury. Moon 12:159–177
Siegler MA, Miller RS, Keane JT, Laneuville M, Paige DA, Matsuyama I, Lawrence DJ, Crotts A, Poston MJ (2016) Lunar true polar wander inferred from polar hydrogen. Nature, 531:480–484
Selkin PA, Tauxe L (2000) Long-term variations in palaeointensity. Philos Trans Roy Soc A 358:1065–1088
Shaar R, Tauxe L (2013) Thellier GUI: An integrated tool for analyzing paleointensity data from Thellier-type experiments. Geochem Geophy Geosyst 14:677–692
Shea EK, Weiss BP, Cassata WS, Shuster DL, Tikoo SM, Gattacceca J, Grove TL, Fuller MD (2012) A long-lived lunar core dynamo. Science 335:453–456
Shimizu H, Matsushima M, Takahashi F, Shibuya H, Tsunakawa H. (2013) Constraint on the lunar core size from electromagnetic sounding based on magnetic field observations by an orbiting satellite. Icarus 222:32–43
Silber RE, Secco RA, Yong W, Littleton JA. (2018) Electrical resistivity of liquid Fe to 12 GPa: Implications for heat flow in cores of terrestrial bodies. Scientific reports 8:1–9
Smith DE, Zuber MT, Neumann GA, Lemoine FG, Mazarico E, Torrence MH, McGarry JF, Rowlands DD, Head JW III, Duxbury TH, Aharonson O, Lucey PG, Robinson MS, Barnouin OS, Cavanaugh JF, Sun X, Liiva P, Mao DD, Smith JC, Bartels AE (2010) Initial observations from the Lunar Orbiter Laser Altimeter (LOLA). Geophys Res Lett 37:L18204
Soderlund KM, King EM, Aurnou JM (2012) The influence of magnetic fields in planetary dynamo models. Earth Planet Sci Lett 333:9–20
Sonett CP (1982) Electromagnetic induction in the Moon. Rev Geophys Space Phys 20:411–455
Sonett CP, Colburn DS, Currie RG (1967) The intrinsic magnetic field of the Moon. J Geophys Res 72:5503–5520
Spohn T, Konrad W, Breuer D, Ziethe R (2001) The longevity of lunar volcanism: Implications of thermal evolution calculations with 2D and 3D mantle convection models. Icarus 149:54–65
Spudis PD, McGovern PJ, Kiefer WS (2013) Large shield volcanoes on the Moon. J Geophys Res 118:1063–1081
Stegman DR, Jellinek AM, Zatman SA, Baumgardnerk JR, Richards MA (2003) An early lunar core dynamo driven by thermochemical mantle convection. Nature 412:143–146
Stephenson A, Collinson DW (1974) Lunar magnetic field paleointensities determined by an anhysteretic remanent magnetization method. Earth Planet Sci Lett 23:220–228
Stevenson DJ (1983) Planetary magnetic fields. Rep Prog Phys 46:555–620
Strangway DW, Sharpe H, Gose W, Pearce G (1973) Magnetism and the interior of the Moon, in Magnetism and Magnetic Materials. American Institute of Physics, New York, pp. 1178–1187
Steenstra ES, Rai N, Knibbe JS, Lin YH, van Westrenen W (2016) New geochemical models of core formation in the Moon from the metal–silicate partitioning of 15 siderophile elements. Earth Planet Sci Lett 441:1–9
Steenstra ES, Lin Y, Rai N, Jansen M, van Westrenen W (2017) Carbon as the dominant light element in the lunar core. Amer Mineral 102:92–97
Stys C, Dumberry M (2020) A past lunar dynamo thermally driven by the precession of its inner core. J Geophys Res 125:e2020JE006396
Suavet C, Weiss BP, Cassata WS, Shuster DL, Gattacceca J, Chan L, Garrick-Bethell I, Head JW, Grove TL, Fuller MD (2013) Persistence and origin of the lunar core dynamo. PNAS 110:8453–8458
Suavet C, Weiss BP, Grove TL (2014) Controlled-atmosphere thermal demagnetization and paleointensity analyses of extraterrestrial rocks. Geochem Geophy Geosyst 15:2733–2743
Sugiura N, Strangway DW (1980) Comparisons of magnetic paleointensity methods using a lunar sample. Proc Lunar Planet Sci Conf 11:1801–1813
Sugiura N, Strangway DW (1983) Magnetic paleointensity determination on lunar sample 62235. Proc Lunar Planet Sci Conf 13:A684-A690
Sugiura N, Strangway DW, Pearce GW (1978) Heating experiments and paleointensity determinations. Proc Lunar Planet Sci Conf 9:3151–3163
Swartzendruber LJ, Itkin, VP, Alcock, CB (1991) The Fe–Ni (iron–nickel) system. J Phase Equilib 12:288–312
Tagle R, Hecht L (2006) Geochemical identification of projectiles in impact rocks. Meteorit Planet Sci 41:1721–1735

Tagle R, Schmitt RT, Erzinger J (2009) Identification of the projectile component in the impact structures Rochechouart, France and Sääksjärvi, Finland: Implications for the impactor population for the Earth. Geochim Cosmochim Acta 73:4891–4906
Takahashi F, Tsunakawa H (2009) Thermal core–mantle coupling in an early lunar dynamo: Implications for a global magnetic field and magnetosphere of the early Moon. Geophys Res Lett 36:L24202
Takahashi F, Tsunakawa H, Shimizu H, Shibuya H, Matsushima M (2014) Reorientation of the early lunar pole. Nat Geosci 7:409–412
Thellier E, Thellier O (1959) Sur l'intensité du champ magnétique terrestre dans le passé historique et géologique. Ann Geophys 15:285–376
Tilgner A (2005) Precession driven dynamos. Phys Fluids 17:034104
Tikoo SM, Weiss BP, Buz J, Lima EA, Shea EK, Melo G, Grove TL (2012) Magnetic fidelity of lunar samples and implications for an ancient core dynamo. Earth Planet Sci Lett 337–338:93–103
Tikoo SM, Weiss BP, Cassata W, Shuster DL, Gattacceca J, Lima EA, Suavet C, Nimmo F, Fuller M (2014) Decline of the lunar core dynamo. Earth Planet Sci Lett 404:89–97
Tikoo SM, Weiss BP, Shuster DL, Suavet C, Wang H, Grove TL (2017) A two-billion-year history for the lunar dynamo. Sci Adv 3:E1700207
Tsunakawa H, Shibuya H, Takahashi F, Shimizu H, Matsushima M, Matsuoka A, Nakazawa S., Otake H, Iijima Y (2010) Lunar magnetic field observation and in situ global mapping of lunar magnetic anomalies by MAP-LMAG onboard SELENE (Kaguya). Space Sci Rev 154:219–251
Tsunakawa H, Takahashi F, Shimizu H, Shibuya H, Matsushima M (2014) Regional mapping of the lunar magnetic anomalies at the surface: Method and its application to strong and weak magnetic anomaly regions. Icarus 228:35–53
Tsunakawa H, Takahashi F, Shimizu H, Shibuya H, Matsushima M (2015) Surface vector mapping of magnetic anomalies over the Moon using Kaguya and Lunar Prospector observations. J Geophys Res 120:1160–1185
Vaughan WM, Head JW, Wilson L, Hess PC (2013) Geology and petrology of enormous volumes of impact melt on the Moon: A case study of the Orientale basin impact melt sea. Icarus 223:749–765
Vervelidou F, Lesur V, Morschhauser A, Grott M, Thomas P (2017) On the accuracy of palaeopole estimations from magnetic field measurements. Geophys J Int 211:1669–1678
Vidal J, Cébron D, Schaeffer N, Hollerbach R (2018) Magnetic fields driven by tidal mixing in radiative stars. Mon Not Roy Astron Soc 475:4579–4594
Ward WR (1975) Past orientation of the lunar spin axis. Science 189:377–379
Watts AW, Greeley R, Melosh HJ (1991) The formation of terrains antipodal to major impacts. Icarus 93:159–168
Weber RC, Lin PY, Garnero EJ, Williams Q, Lognonne P (2011) Seismic detection of the lunar core. Science 331:309–312
Weiss BP, Tikoo SM (2014) The lunar dynamo. Science 346:1198–1209
Whaler KA, Purucker ME (2005) A spatially continuous magnetization model for Mars. J Geophys Res 110:E09001
Wieczorek MA (2018) Strength, depth, and geometry of magnetic sources in the crust of the Moon from localized power spectrum analysis. J Geophys Res 123:291–316
Wieczorek MA, Le Feuvre M (2009) Did a large impact reorient the Moon? Icarus 200:358–366
Wieczorek MA, Phillips RJ (2000) The "Procellarum KREEP Terrane": Implications for mare volcanism and lunar evolution. J Geophys Res 105:20,417–20,430
Wieczorek MA, Zuber MT (2001) A Serenitatis origin for the Imbrian grooves and South Pole–Aitken thorium anomaly. J Geophys Res 106:27,853–27,864
Wieczorek MA, Jolliff BL, Khan A, Pritchard ME B. P. Weiss, Williams JG, Hood LL, Righter K, Neal CR, Shearer CK, McCallum IS, Tompkins S, Hawke BR, Peterson C, Gillis JJ, Bussey B (2006) The constitution and structure of the lunar interior. Rev Mineral Geochem 60:221–364
Wieczorek MA, Weiss BP, Stewart ST (2012) An impactor origin for lunar magnetic anomalies. Science 335:1212–1215
Williams GE (2000) Geological constraints on the Precambrian history of Earth's rotation and the Moon's orbit. Rev Geophys 38:37–59
Williams Q (2009) Bottom-up versus top-down solidification of the cores of small solar system bodies: Constraints on paradoxical cores, Earth Planet Sci Lett 284:564–569
Williams JG, Boggs DH, Yoder CF, Ratcliff JT, Dickey JO (2001) Lunar rotational dissipation in solid body and molten core. J Geophys Res 106:27,933–27,968
Williams JG, Konopliv AS, Boggs DH, Park RS, Yuan D-N, Lemoine FG, Goossens S, Mazarico E, Nimmo F, Weber RC, Asmar SW, Melosh HJ, Neumann GA, Phillips RJ, Smith DE, Solomon SC, Watkins MM, Wieczorek MA, Andrews-Hanna JC, Head JW, Kiefer WS, Matsuyama I, McGovern PJ, Taylor GJ, Zuber MT (2014) Lunar interior properties from the GRAIL mission. J Geophys Res 119:1546–1578
Wu CC, Roberts PH (2013) On a dynamo driven topographically by longitudinal libration. Geophys Astrophys Fluid Dynam 107:20–44
Zhang N, Parmentier EM, Liang Y (2013) A 3-D numerical study of the thermal evolution of the Moon after cumulate mantle overturn: The importance of rheology and core solidification. J Geophys Res 118:1789–1804
Zhang N, Dygert N, Liang Y, Parmentier EM (2017) The effect of ilmenite viscosity on the dynamics and evolution of an overturned lunar cumulate mantle. Geophys Res Lett 44:6543–6552

APPENDIX—RECENT DEVELOPMENTS

Evans AJ, Tikoo SM (2022) An episodic high-intensity lunar core dynamo. Nat Astron 6:325-330

Nichols CIO, Weiss B, Getzin BL, Schmitt HH, Béguin A, Rae ASP, Shah J (2021) The paleo inclination of the ancient lunar magnetic field from an Apollo 17 basalt. Nat Astron 5:1216–1223

Tarduno JA, Cottrell RD, Lawrence K, Bono RK, Huang W, Johnson CL, Blackman EJ, Smirnov AV, Nakajima M, Neal CR, Zhou T, Ibanez-Mejia M, Oda H, Crummins B (2021) Absence of a long-lived lunar paleomagnetosphere. Sci Adv 7:eabi7647

Zhang J, Dumberry M (2021) Viscous dissipation in the fluid core of the Moon. J Geophys Res: Planets 126: e2021JE006966